$^{13}C-^{1}H$ and $^{13}C-^{13}C$ Spin-Coupling Constants in Methyl β-D-Ribofuranoside and Methyl 2-Deoxy-β-D-*erythro*-pentofuranoside: Correlations with Molecular Structure and Conformation

Timothy J. Church,[†] Ian Carmichael,[‡] and Anthony S. Serianni*[,†]

Contribution from the Department of Chemistry and Biochemistry, and Radiation Laboratory, University of Notre Dame, Notre Dame, Indiana 46556

Received January 24, 1997. Revised Manuscript Received June 11, 1997[⊗]

Abstract: Methyl β-D-ribofuranoside **5** and methyl 2-deoxy-β-D-*erythro*-pentofuranoside (methyl 2-deoxy-β-D-ribofuranoside) **6** were synthesized with single sites of ^{13}C-enrichment at each carbon, and a complete set of $^{13}C-^{1}H$ and $^{13}C-^{13}C$ spin-coupling constants (37 couplings in **5**, 41 couplings in **6**) in these molecules were obtained by 1D and 2D NMR spectroscopy. $^{2}J_{CH}$ coupling signs were determined from the observation of relative cross-peak displacements in 2D TOCSY data. The $^{13}C-^{1}H$ couplings (one-, two-, and three-bond) were interpreted in structural and conformational terms with assistance from conformational models of **5** and **6** based on conventional two-state pseudorotational analysis of $^{3}J_{HH}$ values (PSEUROT) and on theoretical predictions of conformational energies and J_{CH} values obtained from *ab initio* molecular orbital calculations on the ten envelope and planar conformers of β-D-ribofuranose **4** and 2-deoxy-β-D-*erythro*-pentofuranose (2-deoxy-β-D-ribofuranose) **3**. A comparison of theoretical J_{CH} values in **3** and **4** allowed an assessment of the effect of C2 structure (C2 oxy *vs* C2 deoxy) on coupling magnitudes and signs. Results show that the behavior of related J_{CH} values in **5** and **6** may differ, especially when C2 is involved as a coupled nucleus. In addition, several $^{1}J_{CH}$, $^{2}J_{CH}$, and $^{3}J_{CH}$ values in β-D-*ribo* and 2-deoxy-β-D-*ribo* rings were found to be sensitive to furanose ring and hydroxymethyl group conformation; in the deoxy*ribo* ring, the presence of diastereotopic protons at C2 produces paired $^{13}C-^{1}H$ coupling pathways involving H2*R* and H2*S* that are complementary, and differences in the resulting paired J_{CH} values are, in some instances, sensitive to ring conformation. J_{CC} values in β-D-*ribo* and 2-deoxy-β-D-*ribo* rings also reflect differences in ring structure and geometry, although fewer (*e.g.*, $^{2}J_{C3,C5}$, $^{3}J_{C1,C5}$, $^{3}J_{C2,C5}$) appear useful as conformational probes. The correlations drawn between ring structure/conformation and J_{CH}/J_{CC} magnitude and sign in **5** and **6** will be useful in anticipated applications of these couplings to assess furanose ring conformation/dynamics in DNA and RNA oligomers and in other biomolecules containing β-D-*ribo* and 2-deoxy-β-D-*ribo* rings.

Introduction

$^{13}C-^{1}H$ and $^{13}C-^{13}C$ spin-coupling constants are becoming more important in biomolecular structure determinations by NMR spectroscopy, in part due to the increased availability of ^{13}C-labeled samples and to improved methods to measure these parameters in complex molecules. Thus, for example, $^{3}J_{CH}$ and $^{3}J_{CC}$ values have been used to refine NMR structure determinations of ^{13}C-labeled proteins, especially for the side chains.[1−3] $^{1}J_{CH}$ values have also been examined as potential probes of protein backbone conformation.[4−7] $^{1}J_{CH}$, $^{3}J_{CH}$, and $^{3}J_{CC}$ values have proven valuable in the conformational analysis of complex carbohydrates, especially when assessing conformation about *O*-glycoside linkages.[8−14] J_{CH} values can be conveniently measured by a variety of multidimensional NMR methods;[2] for example, an elegant approach involves the measurement of cross-peak displacements in 2D (*e.g.*, TOCSY)[15,16] and 3D (*e.g.*, HMQC-TOCSY)[17] spectra of ^{13}C-labeled molecules, from which both the magnitudes and signs of specific J_{CH} may be obtained.[2,3a,18,19] Recent improvements in the ^{13}C-labeling of DNA[20] and RNA[21] promise increased measurement and ap-

* Author for correspondence.
† Department of Chemistry and Biochemistry.
‡ Radiation Laboratory.
⊗ Abstract published in *Advance ACS Abstracts,* August 15, 1997.

(1) Schmieder, P.; Kurz, M.; Kessler, H. *J. Biomol. NMR* **1991**, *1*, 403−420.
(2) Biamonti, C.; Rios, C. B.; Lyons, B. A.; Montelione, G. T. *Adv. Biophys. Chem.* **1994**, *4*, 51−120.
(3) (a) Montelione, G. T.; Winkler, M. E.; Rauenbuehler, P.; Wagner, G. *J. Magn. Reson.* **1989**, *82*, 198−204. (b) Hu, J.-S.; Bax, A. *J. Am. Chem. Soc.* **1996**, *118*, 8170−8171.
(4) Egli, H.; von Philipsborn, W. *Helv. Chim. Acta* **1981**, *64*, 976−988.
(5) Mierke, D. F.; Grdadolnik, S. G.; Kessler, H. *J. Am. Chem. Soc.* **1992**, *114*, 8283−8284.
(6) Vuister, G. W.; Delaglio, F.; Bax, A. *J. Am. Chem. Soc.* **1992**, *114*, 9674−9675.
(7) Vuister, G. W.; Delaglio, F.; Bax, A. *J. Biomol. NMR* **1993**, *3*, 67−80.
(8) Excoffier, G.; Gagnaire, D. Y.; Taravel, F. R. *Carbohydr. Res.* **1974**, *56*, 229.
(9) Nunez, H. A.; Barker, R. *Biochemistry* **1980**, *19*, 489.
(10) Hayes, M. L.; Serianni, A. S.; Barker, R. *Carbohydr. Res.* **1982**, *100*, 87.
(11) Duker, J.; Serianni, A. S. *Carbohydr. Res.* **1993**, *249*, 281.
(12) (a) Tvaroska, I. *Carbohydr. Res.* **1990**, *206*, 55. (b) Tvaroska, I.; Taravel, F. R. *Carbohydr. Res.* **1991**, *221*, 83−94. (c) Tvaroska, I.; Taravel, F. R. *J. Biomol. NMR* **1992**, *2*, 421−430.
(13) Church, T.; Carmichael, I.; Serianni, A. S. *Carbohydr. Res.* **1996**, *280*, 177−186.
(14) Hricovini, M.; Tvaroska, I. *Magn. Reson. Chem.* **1990**, *28*, 862−866.
(15) Braunschweiler, L.; Ernst, R. R. *J. Magn. Reson.* **1983**, *53*, 521−528.
(16) Bax, A.; Davis, D. G. *J. Magn. Reson.* **1985**, *65*, 355−360.
(17) Wijmenga, S. S.; Hallenga, K.; Hilbers, C. W. *J. Magn. Reson.* **1989**, *84*, 634−642.
(18) Serianni, A. S.; Podlasek, C. A. *Carbohydr. Res.* **1994**, *259*, 277−282.
(19) Hines, J. V.; Landry, S. M.; Varani, G.; Tinoco, I., Jr. *J. Am. Chem. Soc.* **1994**, *116*, 5823−5831.

S0002-7863(97)00231-X CCC: $14.00

Chart 1

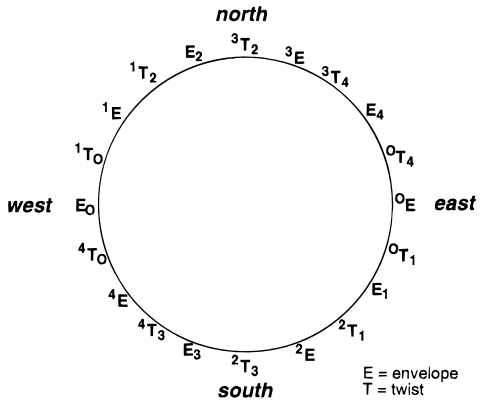

Pseudorotational itinerary of an aldofuranose ring

plications of J_{CH} and J_{CC} values in NMR structural studies of nucleic acids.

While suitable labeled samples and NMR methodologies exist to extract accurate J_{CH} and J_{CC} values from NMR spectra of biomolecules, relating their magnitudes to molecular structure is often difficult. The problem is most acute in studies of nucleic acids, especially for couplings within the sugar (furanose) constituent. Because of the inherent conformational flexibility of the furanose ring,[22] *J* values observed in these structures cannot be interpreted in terms of a single rigid conformation but rather are averaged[23] in a manner that reflects the presence of a mixture of two or more interconverting conformational isomers.[24a] Pathways for conformer interconversion involve pseudorotation[24b] in which envelope (E) and twist (T) nonplanar forms exchange without the participation of the planar (P) form (Chart 1), or inversion[24c] in which nonplanar forms interconvert via the P form. This conformational averaging provides a strong justification for improving the interpretation of J_{CH} and J_{CC} within these structures.[25,26a] Given the large number of J_{CH} and J_{CC} values relative to J_{HH} values in β-D-*ribo* **1** and 2-deoxy-β-D-*ribo* **2** rings (Chart 2), these couplings represent an important potential source of information with which to assess the conformational and dynamical properties of these rings. Thus, an integrated, quantitative treatment of J_{HH}, J_{CH}, and J_{CC} values within the furanose constituents of DNA and RNA, and other biomolecules that contain these rings,[26b] is expected to lead to a fuller understanding of their solution behaviors.

Previous reports have addressed the effect of furanose ring conformation on $^1J_{CH}$ values and suggest a correlation between C−H bond orientation, C−H bond length, and coupling magnitude.[27,28] A projection resultant method has been proposed recently to assist in the interpretation of $^2J_{CC}$ values in carbohydrates;[13] this method was subsequently confirmed by magnitude and sign determinations of $^2J_{CCC}$ and $^2J_{COC}$ values by ^{13}C−^{13}C β-COSY methods using triply ^{13}C-labeled compounds.[29] A detailed investigation of J_{CH} behavior in β-D-ribofuranosyl rings has also been reported recently in which the effect of ring conformation on $^1J_{CH}$, $^2J_{CH}$, and $^3J_{CH}$ values was examined using experimental and computational methods.[28]

Chart 2

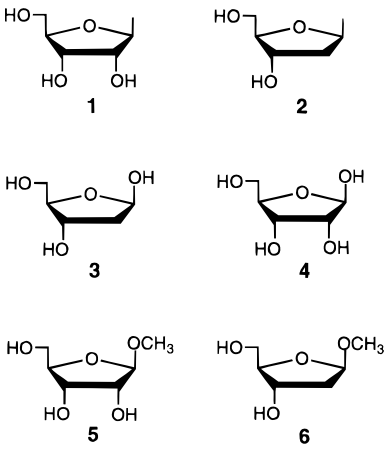

In the present investigation, we extend these previous studies by examining J_{CH} and J_{CC} behavior in the 2-deoxy-β-D-ribofuranosyl ring **2** (Chart 2). We compare the structural properties of 2-deoxy-β-D-*erythro*-pentofuranose (2-deoxy-β-D-ribofuranose) **3** (Chart 2) derived from *ab initio* molecular orbital calculations to those obtained previously[27,28,30] on β-D-ribofuranose **4** (Chart 2). Using computational methods validated previously,[27,28,30,31] we then compare the predicted (computed) behavior of J_{CH} values in **3** with that predicted for related J_{CH} in **4**; this latter comparison provides an estimation of the effect of C2 structure (C2 oxy *vs* C2 deoxy) on J_{CH} values. We then apply this comparative analysis in a discussion of the complete sets of J_{CH} and J_{CC} values observed in methyl β-D-ribofuranoside **5** (37 couplings) and methyl 2-deoxy-β-D-*erythro*-pentofuranoside (methyl 2-deoxy-β-D-ribofuranoside) **6** (41 couplings) (Chart 2). These couplings were obtained from 1D and 2D NMR spectra of **5** and **6** which were singly labeled with ^{13}C at each carbon.

Experimental Section

Synthesis of Labeled Methyl β-D-Ribofuranosides. Singly ^{13}C-labeled D-riboses were prepared according to previously published procedures,[32−36] and only a brief account of their synthesis is given here. D-[1-^{13}C]Ribose was prepared from D-erythrose[37] and K^{13}CN by the cyanohydrin reduction reaction;[32,33,35] the product C-2 epimers, D-[1-^{13}C]ribose and D-[1-^{13}C]arabinose, were separated by chromatography on Dowex 50 × 8 (200−400 mesh) ion-exchange resin in the Ca^{2+} form.[38] D-[2-^{13}C]Ribose was prepared from D-[1-^{13}C]arabinose (the

(20) (a) Lancelot, G.; Chanteloup, L.; Beau, J. M.; Thuong, N. T. *J. Am. Chem. Soc.* **1993**, *115*, 1599. (b) Sklenar, V.; Peterson, R. D.; Rejante, M. R.; Feigon, J. *J. Biomol. NMR* **1993**, *3*, 721. (c) Ono, A.; Tate, S.; Kainosho, M. *J. Biomol. NMR* **1994**, *4*, 581−586. (d) Wu, J.; Serianni, A. S. *Biopolymers* **1994**, *34*, 1175−1186. (e) Zimmer, D. P.; Crothers, D. M. *Proc. Natl. Acad. Sci. U.S.A.* **1995**, *92*, 3091−3095.

(21) Nikonowicz, E. P.; Sirr, A.; Legault, P.; Jucker, F. M.; Baer, L. M.; Pardi, A. *Nucl. Acids Res.* **1992**, *20*, 4507−4513.

(22) Harvey, S. C.; Prabhakaran, M. *J. Am. Chem. Soc.* **1986**, *108*, 6128−6136.

(23) Jardetzky, O. *Biochem. Biophys. Acta* **1980**, *621*, 227−232.

(24) (a) Olson, W. K. *J. Am. Chem. Soc.* **1982**, *104*, 278−286. (b) Altona, C.; Sundaralingam, M. *J. Am. Chem. Soc.* **1972**, *94*, 8205−8212. (c) Westhof, E.; Sundaralingam, M. *J. Am. Chem. Soc.* **1983**, *105*, 970−976.

(25) Cyr, N.; Perlin, A. S. *Can. J. Chem.* **1979**, *57*, 2504.

(26) (a) Serianni, A. S.; Barker, R. *J. Org. Chem.* **1984**, *49*, 3292−3300. (b) Cicero, D. O.; Barbato, G.; Bazzo, R. *Tetrahedron* **1995**, 51, 10303−10316.

(27) Serianni, A. S.; Wu, J.; Carmichael, I. *J. Am. Chem. Soc.* **1995**, *117*, 8645−8650.

(28) Podlasek, C. A.; Stripe, W. A.; Carmichael, I.; Shang, M.; Basu, B.; Serianni, A. S. *J. Am. Chem. Soc.* **1996**, *118*, 1413−1425.

(29) Serianni, A. S.; Bondo, P. B.; Zajicek, J. *J. Magn. Reson. Ser. B* **1996**, *112*, 69−74.

(30) Carmichael, I.; Chipman, D. M.; Podlasek, C. A.; Serianni, A. S. *J. Am. Chem. Soc.* **1993**, *115*, 10863−10870.

(31) Carmichael, I. *J. Phys. Chem.* **1993**, *97*, 1789−1792.

(32) Serianni, A. S.; Nunez, H. A.; Barker, R. *Carbohydr. Res.* **1979**, *72*, 71−78.

(33) Serianni, A. S.; Clark, E. L.; Barker, R. *Carbohydr. Res.* **1979**, *72*, 79−91.

(34) Serianni, A. S.; Vuorinen, T.; Bondo, P. B. *J. Carbohydr. Chem.* **1990**, *9*, 513−541.

(35) Serianni, A. S.; Bondo, P. B. *J. Biomol. Struct. Dyn.* **1994**, *11*, 1133−1148.

byproduct in the synthesis of D-[1-^{13}C]ribose) by molybdate-catalyzed epimerization.[35,36] D-[3-^{13}C]Ribose was prepared from D-[2-^{13}C]erythrose and KCN by the cyanohydrin reduction reaction;[32,33,35] D-[2-^{13}C]-erythrose was prepared by molybdate epimerization[36] of D-[1-^{13}C]-threose, and the latter labeled tetrose was prepared from D-glyceraldehyde[39] and K^{13}CN.[33] D-[4-^{13}C]Ribose was prepared from D-[2-^{13}C]mannose;[40] the labeled mannose was prepared by molybdate epimerization of D-[1-^{13}C]glucose,[36] and the labeled glucose was prepared from D-arabinose and K^{13}CN.[32−34] D-[5-^{13}C]Ribose was prepared from D-[4-^{13}C]erythrose and KCN by the cyanohydrin reduction reaction;[32,33,35] D-[4-^{13}C]erythrose was prepared by treatment of D-[6-^{13}C]glucose[41] with $Pb(OAc)_4$.[37]

The labeled riboses were converted into the corresponding methyl furanosides by Fischer glycosidation (anhydrous methanol solvent, H_2SO_4 catalyst).[42,43] The product α- and β-furanosides were separated by chromatography on Dowex 1 × 2 (200−400 mesh) ion-exchange resin in the OH^- form.[43,44]

Synthesis of Labeled Methyl 2-Deoxy-β-D-*erythro*-pentofuranosides. Labeled methyl 2-deoxy-β-D-*erythro*-pentofuranosides (methyl 2-deoxy-β-D-ribofuranosides) were prepared from the corresponding labeled methyl β-D-ribofuranosides according to the method of Robins *et al.*[45] A general description of the procedure, as applied to the preparation of methyl 2-deoxy-β-D-[1-^{13}C]*erythro*-pentofuranoside, follows.

Methyl β-D-[1-^{13}C]ribofuranoside (0.54 g, 3.3 mmol) was suspended in dry pyridine (40 mL; freshly distilled and stored over 3Å molecular sieves) in an inert (N_2) atmosphere. 1,3-Dichloro-1,1,3,3-tetraisopropyldisiloxane (TPDS-Cl_2, 1.07 mL, 3.3 mmol) was added, and the mixture was stirred at room temperature for 5 h. Pyridine was removed by evaporation *in vacuo*, and the residue was partitioned betweeen EtOAc and water. The organic phase was washed with 3 × 30 mL saturated $NaHCO_3$ and once with saturated aqueous NaCl, and the organic phase was dried overnight over anhydrous Na_2SO_4.

The solvent was removed by evaporation *in vacuo*, and anhydrous CH_3CN (45 mL), 4-(dimethylamino)pyridine (DMAP, 825 mg, 6.6 mmol), and phenylthionocarbonate chloride (PTC-Cl, 0.6 mL, 3.3 mmol) were added. The solution was stirred for 21 h under an inert atmosphere (N_2). Solvent was then removed by evaporation *in vacuo*, and the residue was partitioned between EtOAc and water. The organic phase was washed with 3 × 30 mL saturated $NaHCO_3$ and once with saturated aqueous NaCl, and the organic phase was dried overnight over anhydrous Na_2SO_4.

After removal of the solvent *in vacuo*, the resulting syrup was dissolved in toluene (80 mL, freshly distilled and stored over 3Å molecular sieves), and 2,2′-azobis(2-methylpropionitrile) (AIBN, 0.11g, 0.7 mmol) and tri-*n*-butyltin hydride (1.2 mL, 4.5 mmol) were added. The solution was degassed with O_2-free nitrogen for 1 h and then heated at 75 °C for 6 h. Deprotection (desilylation) was effected by addition of tetra-*n*-butylammonium fluoride (TBAF, 6 mL, 6 mmol) to the reaction mixture, and the solution was heated at 75° C for an additional 3 h. Solvent was then removed by evaporation *in vacuo*, and the residue partitioned between ether and water. The ether layer was extracted with 3 × 20 mL of water, and the aqueous fractions were pooled and extracted with 3 × 20 mL of ether. The resulting aqueous phase was concentrated *in vacuo* at 30 °C, and the resulting syrup applied to a column (2.5 cm × 26 cm) containing Dowex 1 × 2 (200−400 mesh) resin in the OH^- form.[44] Elution with CO_2-free water (2 mL/min, 15 mL/fraction) yielded methyl 2-deoxy-β-D-[1-^{13}C]*erythro*-pentofuranoside (120−255 mL) and methyl β-D-[1-^{13}C]ribofuranoside (450−750 mL), which were identified by their characteristic ^{1}H chemical shifts and ^{1}H−^{1}H coupling constants.[43,46] Yield: 0.30 g, 2.0 mmol, 61% (syrup weight) based on methyl β-D-[1-^{13}C]ribofuranoside.

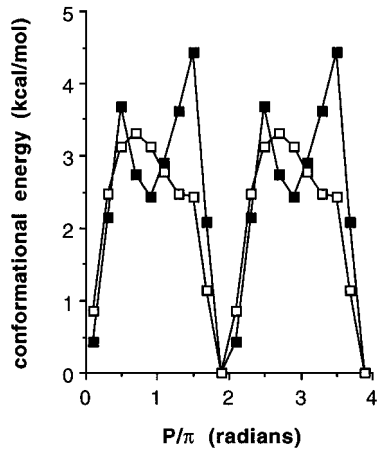

Figure 1. Conformational energy (total energy) profiles for 2-deoxy-β-D-*erythro*-pentofuranose **3** (open squares) and β-D-ribofuranose **4** (closed squares) determined from *ab initio* molecular orbital calculations (HF/6-31G*) using the initial C1−O1, C2−O2 (*ribo* only), C3−O3, C4−C5, and C5−O5 torsion angles shown in Chart 3.

NMR Spectroscopy. NMR spectra were obtained on a Varian Unity*Plus* 600 MHz NMR spectrometer operating at 599.888 MHz for ^{1}H and 150.852 MHz for ^{13}C. One-dimensional ^{1}H and ^{13}C NMR spectra were collected on ∼20 and ∼100 mM aqueous (^2H_2O) solutions, respectively, at 30 °C using a conventional 5 mm broadband probe or a 3 mm dual ^{1}H/^{13}C microprobe (Nalorac). Spectra were processed with resolution enhancement (sine-bell) to facilitate the measurement of small couplings (≥0.8 Hz). 2D TOCSY spectra[15,16] were collected as a 2K × 2K matrix and zerofilled to 4K × 4K, and a 50 ms mixing time was employed in the pulse sequence. Sine-bell functions were applied to both dimensions prior to fourier transformation. 2D Spectra were sufficiently digitized to observe relative cross-peak displacements >1 Hz; these data were used only for sign determinations, since accurate coupling magnitudes (±0.1 Hz) could be extracted straightforwardly from 1D ^{1}H NMR spectra in most cases.

$^3J_{HH}$ values were fit to a two-state N/S pseudorotational model using PSEUROT 6.2,[47] which applies a parameterized Karplus equation[48] to the coupling data and yields pseudorotational phase angles (*P*) and puckering amplitudes (τ_m) for the preferred north (N) and south (S) forms, and the percentage of S form in solution. Pseudorotational phase angles (*P*) divided by π give values ranging from 0−2 radians which correspond to specific E and T forms (*e.g.*, $P/\pi = 0.1$ for ^{3}E, $P/\pi = 0.3$ for E_4, and so forth) (Figure 1).

***Ab Initio* Molecular Orbital Calculations.** *Ab initio* molecular orbital (MO) calculations were conducted (Gaussian 92)[49] on 2-deoxy-β-D-*erythro*-pentofuranose **3** using the Hartree−Fock (HF) procedure and a polarized split-valence basis set (6-31G*). Ten envelope conformers (^{3}E, E_4, ^{0}E, E_1, ^{2}E, E_3, ^{4}E, E_0, ^{1}E, E_2) (Chart 1) and the planar (P) conformer were examined as described previously[27,28,50−52] by constraining appropriate endocyclic torsion angles within **3** to 0°

(36) Hayes, M. L.; Pennings, N. J.; Serianni, A. S.; Barker, R. *J. Am. Chem. Soc.* **1982**, *104*, 6764−6769.
(37) Perlin, A. S. *Methods Carbohydr. Chem.* **1962**, *1*, 64−66.
(38) Angyal, S. J.; Bethell, G. S.; Beveridge, R. *Carbohydr. Res.* **1979**, *73*, 9−18.
(39) Perlin, A. S. *Methods Carbohydr. Chem.* **1962**, *1*, 61−63.
(40) Wu, J.; Serianni, A. S.; Bondo, P. B. *Carbohydr. Res.* **1992**, *226*, 261−269.
(41) King-Morris, M. J.; Bondo, P. B.; Mrowca, R. A.; Serianni, A. S. *Carbohydr. Res.* **1988**, *175*, 49−58.
(42) Barker, R.; Fletcher, H. G., Jr. *J. Org. Chem.* **1961**, *26*, 4605.
(43) Kline, P. C.; Serianni, A. S. *J. Am. Chem. Soc.* **1990**, *112*, 7373−7381.
(44) Austin, P. W.; Hardy, F. E.; Buchanan, J. C.; Baddiley, J. *J. Chem. Soc.* **1963**, 5350-5353.
(45) Robins, M. J.; Wilson, J. S.; Hansske, F. *J. Am. Chem. Soc.* **1983**, *105*, 4059.
(46) Raap, J.; van Boom, J. H.; van Lieshout, H. C.; Haasnoot, C. A. G. *J. Am. Chem. Soc.* **1988**, *110*, 2736−2743.
(47) PSEUROT 6.2; Gorlaeus Laboratories: University of Leiden.
(48) Haasnoot, C. A. G.; de Leeuw, F. A. A. M.; Altona, C. *Tetrahedron* **1980**, *36*, 2783.
(49) Frisch, M. J.; Trucks, G. W.; Head-Gordon, M.; Gill, P. M. W.; Wong, M. W.; Foresman, J. B.; Johnson, B. G.; Schlegel, H. B.; Robb, M. A.; Replogle, E. S.; Gomperts, R.; Andres, J. L.; Raghavachari, K.; Binkley, J. S.; Gonzales, C.; Martin, R. L.; Fox, D. J.; DeFrees, D. J.; Baker, J.; Stewart, J. J. P.; Pople, J. A. Gaussian 92, Revision C.3; Gaussian, Inc.: Pittsburgh, PA, 1992.
(50) Serianni, A. S.; Chipman, D. M. *J. Am. Chem. Soc.* **1987**, *109*, 5297.
(51) Garrett, E. C.; Serianni, A. S. In *Computer Modeling of Carbohydrate Molecules*; French, A. D., Brady, J. W., Eds.; ACS Symposium Series 430; American Chemical Society: Washington, DC, 1990; pp 91−119.

Chart 3

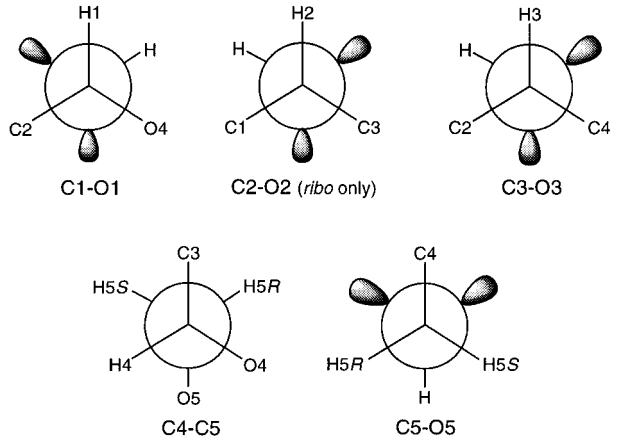

(thus, for example, in ^{3}E, the C4−O4−C1−C2 dihedral angle was fixed at 0°); two endocyclic torsions were fixed at 0° in calculations on the P form. All other geometric parameters (*i.e.*, bond lengths, angles, and torsions) were optimized in the calculations.

The choice of initial exocyclic C−C and C−O torsions (C1−O1, C3−O3, C4−C5, and C5−O5 in **3**) (Chart 3) was arbitrary except for the C1−O1 torsion, which was set to optimize the exoanomeric effect,[53] as described in previous reports,[27,28,50−52] and the C4−C5 torsion angle. The latter torsion angle was set to correspond to the hydroxymethyl conformation favored by **5** and **6** in aqueous solution (C3 *anti* to O5; *gt* conformer; Chart 3) (see Results and Discussion) in order to permit a comparison between experimental and computed J_{CH} values in these structures. Thus, the full energy surface for **3** was not examined since, to obtain this surface, $3^4 \times 11 = 891$ unique structures would need to be studied, which was considered impractical given present computer limitations. It should also be appreciated that these calculations pertain to unsolvated, "gas-phase" structures (*i.e.*, solvent effects have not been treated), since at present it is not possible to include solvation effects, either implicitly by a suitably configured dielectric reaction-field or explicitly by selecting and locating a suitable number of solvent molecules, in such *ab initio* calculations with reasonable confidence.

Calculation of ^{13}C−^{1}H Spin-Coupling Constants. ^{13}C−^{1}H spin-coupling constants were obtained by finite (Fermi-contact) field double perturbation theory calculations[54a] at the HF and MP2 levels using a basis set designed for the economical recovery of such properties and a modified version of the Gaussian 92 suite of programs.[31] Scale factors have been developed for this basis set for each of the spin-coupling constants, $^1J_{CH}$, $^2J_{CH}$, and $^3J_{CH}$, which allow the reliable prediction of results expected at a much higher level of theory, namely, quadratic configuration interaction (QCISD).[54b] The scale factors were estimated from the equation, $f_n = [^nJ_{CH}(\text{QCISD}) - {}^nJ_{CH}(\text{HF})]/[^nJ_{CH}(\text{MP2}) - {}^nJ_{CH}(\text{HF})]$, in systems where the full QCISD calculation is possible. Values of $f_1 = 0.83$, $f_2 = 0.75$, and $f_3 = 0.83$ were obtained for the present basis set which is derived from standard double-zeta representations and may be written as [5*s*2*p*1*d*|2*s*].[31] Note the presence of a shell of five-component, polarizing *d*-functions on the heavy atoms (C,O). The addition of *p*-functions on hydrogen produced little change in the computed couplings. These values allow the estimation of $^nJ_{CH}$ (QCISD) values in much larger systems for which only the HF and MP2 calculations are at present tractable. It should be observed that *trends* in the computed coupling constants are already reproduced at the HF level, whereas the *absolute magnitudes* are poorly estimated due to the neglect of electron correlation. The importance of these electron correlation effects is overestimated in the simplest recovery scheme (MP2), so that the comparison with much more complete treatments (QCISD) leads to scale factors less than unity.

(52) Garrett, E. C.; Serianni, A. S. *Carbohydr. Res.* **1990**, *206*, 183.
(53) (a) Lemieux, R. A. *Pure Appl. Chem.* **1971**, *25*, 527−548. (b) Lemieux, R. U.; Koto, S.; Voisin, D. In *Anomeric Effect: Origin and Consequences*; Szarek, W. A., Horton, D., Eds.; ACS Symposium Series 87; American Chemical Society: Washington, DC, 1979; pp 17−29.
(54) (a) Kowalewski, J.; Laaksonen, A.; Roos, B.; Siegbahn, P. *J. Chem. Phys.* **1979**, *71*, 2896−2902. (b) Pople, J. A.; Head-Gordon, M.; Raghavachari, K. *J. Chem. Phys.* **1987**, *87*, 5968−5975.

Table 1. ^{1}H Chemical Shifts and ^{1}H−^{1}H Spin-Coupling Constants in Methyl β-D-ribofuranoside **5** and Methyl 2-Deoxy-β-D-ribofuranoside **6**

chemical shifts, δ^a (ppm)	**5**	**6**
H1	4.977	5.310
H2	4.114	
H2*R*		2.248
H2*S*		2.316
H3	4.236	4.438
H4	4.092	4.076
H5*R*	3.690	3.678
H5*S*	3.876	3.794
OCH_3	3.480	3.477
coupling constants, J^a (Hz)	**5**^{b}	**6**
H1,H2	1.2	
H1,H2*R*		5.4
H1,H2*S*		2.6
H2,H3	4.6	
H2*R*,H3		∼5.7
H2*S*,H3		6.7
H2*R*,H2*S*		−13.9
H3,H4	6.9	4.2
H4,H5*R*	6.6	7.0
H4,H5*S*	3.1	4.6
H5*R*,H5*S*	−12.2	−12.0

^{a} ^2H_2O solvent, ∼25 °C. ^{b} Data taken from ref 43.

Chart 4

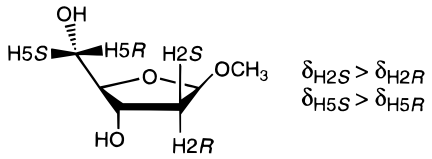

Results and Discussion

A. Ring and Hydroxymethyl Conformations in 5 and 6 via Analysis of $^3J_{HH}$ Values. ^{1}H NMR spectra of **5** and **6** obtained at 600 MHz in ^2H_2O solvent contained well-resolved signals for the nonexchangeable protons, thus allowing straightforward extraction of chemical shifts and $^3J_{HH}$ values from the data (Table 1). The stereochemical assignments of the diastereotopic C2 proton signals of **6** (H2*R*, H2*S*) could not be made reliably from an inspection of $^3J_{HH}$ data due to potential complications arising from conformational averaging. However, these assignments could be made with confidence based on an analysis of $^2J_{C1,H2R}$ and $^2J_{C1,H2S}$ values as discussed below; using this approach, the more shielded C2 proton was assigned as H2*R* (the C2 proton *cis* to O3) (Table 1, Chart 4). Stereochemical assignments of the hydroxymethyl protons (H5*R*, H5*S*) in **5** were made previously through selective deuterium substitution;[55a] the more shielded C5 proton is H5*R* (Table 1, Chart 4). By analogy, the more shielded C5 proton in **6** was initially assigned to H5*R* and subsequently confirmed by analysis of J_{CH} values (see below).

$^3J_{HH}$ data for **5** and **6** were analyzed by PSEUROT 6.2[47] which fits these couplings to a simple two-state north/south (N/S) conformational model. Pseudorotational phase angles for the preferred N and S forms (P_N and P_S, respectively), puckering amplitudes for these forms (τ_m(N) and τ_m(S), respectively), and the %S form in solution are obtained from this treatment. The PSEUROT results (Table 2) indicate a strong preference for N forms by methyl β-D-ribofuranoside **5** ($P_N = -16°$, $P_S = 158°$; $\tau_m(N) = 38°$, $\tau_m(S) = 42°$, N/S = 94/6). In contrast, treatment of $^3J_{HH}$ data for **6** gave $P_N = -26°$, $P_S = 211°$, $\tau_m(N) = 38°$, $\tau_m(S) = 32°$, and N/S = 60/40. Thus, according to this treatment, the preferred N forms of **5** and **6** are similar (*i.e.*, $^1T_2/E_2$), whereas the preferred S forms differ considerably (^{2}E

Table 2. PSEUROT 6.2[a] Parameters for Methyl β-D-ribofuranoside **5** and Methyl 2-Deoxy-β-D-ribofuranoside **6** Based on $^3J_{HH}$ Data[c]

parameter[b]	**5**	**6**
P_N	−16° (E_2)	−26° ($E_2/{}^1T_2$)
P_S	158° (^2E)	211° ($^4T_3$)
τ_m (N)	38°	38°
τ_m (S)	42°	32°
N/S ratio	94/6	60/40
RMS deviation[d]	0.00	0.31

[a] Original program description, ref 74; program source, ref 47. [b] ^2H_2O solvent, ∼25 °C. [c] Coupling data provided in Table 1. [d] In Hz.

Chart 5

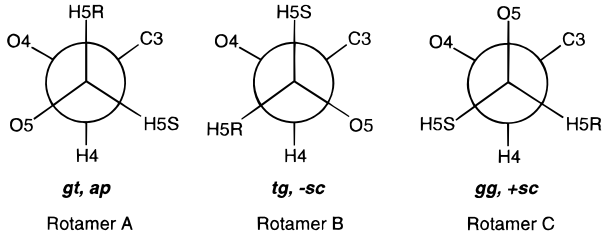

for **5**, $^4T_3$ for **6**). The PSEUROT data obtained for **6** are in good agreement with those reported previously by Raap *et al.*[46]

Hydroxymethyl conformation in **5** and **6** has been examined previously.[55a−c] Populations for the three C4−C5 rotamers (Chart 5) were calculated from the magnitudes of $^3J_{H4,H5R}$ and $^3J_{H4,H5S}$ values (Table 3).[55b] These results indicate very similar populations (52%) of the *gt* rotamer in both **5** and **6**. The populations of the *gg* (38%) and *tg* (10%) rotamers are significantly different in **5**, whereas these populations are similar (21% and 26%, respectively) in **6**. The smaller *tg* population in **5** relative to that found in **6** is apparently related to a greater preference for N forms in the former;[55b] in N forms, a destabilizing 1,3-interaction exists between O3 and O5 in the *tg* rotamer, thus reducing its population in solution.

B. Molecular Orbital Calculations on 2-Deoxy-β-D-ribofuranose 3 and Comparisons to Related Data for 4. *Ab initio* molecular orbital calculations were performed on **3** to evaluate conformational energy and structural parameters as a function of ring conformation. Similar calculations were reported recently on **4**.[28] In the following discussion, data for **3** and **4** are compared in order to assess the effect of C2 structure on conformational energies and structural parameters.

Previous conformational energy studies of **4** conducted at the same level of theory used in this study (HF/6-31G*) revealed two energy minima along the pseudorotational itinerary;[28] the global minimum occurred at 1.9 P/π (E_2, N form) and a local minimum at 0.9 P/π (^2E, S form) (Chart 1, Figure 1). The more favored N form was found to be structurally similar to the two conformations of the corresponding methyl glycoside **5** observed in the crystalline state.[28] Similar calculations on **3** also reveal two minima, with the global minimum located at 1.9 P/π (E_2, N form) and a barely discernable local minimum at about 1.3*P*/π (^4E) (Figure 1). Thus, based on these data, the E_2 conformation appears to be the most favored N form of both **3** and **4**, whereas the preferred S forms of **3** and **4** differ. These results are consistent with those obtained from the treatment of $^3J_{HH}$ values in the structurally related glycosides **5** and **6** (Table 2), that is, *similar preferred N and S forms are identified by $^3J_{HH}$ analysis and by ab initio calculations.* However, the proportions of N and S forms determined by the two methods differ, and we attribute this discrepancy, in part, to the limitations imposed by restricting the *ab initio* calculations to one set of exocyclic torsion angles (Chart 3). Thus, for example, the fact that only the *gt* conformation about the C4−C5 bond (Chart 5) was considered is likely to skew the N/S distribution more in favor of N forms in these computations; inclusion of *gg* and *tg* rotamers is expected to increase the percentage of S forms for reasons discussed elsewhere.[55b] The exclusion of solvent water in the present calculations may also affect the computed N/S ratios.

C−H bond lengths in **3** and **4** show the same general dependence on ring conformation (Figure 2). The C1−H1 bond is longer in conformations in which this bond is quasi-axial or near quasi-axial (*e.g.*, E_1) and shorter in conformations in which this bond is quasi-equatorial or near quasi-equatorial (*e.g.*, ^1E) (Figure 2A). Similar patterns are observed for the C2−H2 and C4−H4 bonds in **3** and **4** (Figures 2B,C) and are consistent with observations made previously on simpler 2-deoxyaldofuranoses.[27,51] In contrast, the behavior of the C3−H3 bond length in **3** and **4** differs (Figure 2D). In **3**, the behavior of the C3−H3 bond is consistent with previous observations,[27,28] that is, the bond is longer when quasi-axial or near quasi-axial (*e.g.*, ^3E) and shorter when quasi-equatorial or near quasi-equatorial (*e.g.*, E_3). Thus, the behavior of the C3−H3 bond in **4** is anomalous and has been attributed to changes in the C3−O3 torsion angle as the *ribo* ring is optimized in different conformations.[27,28] The large rotation of the C3−O3 bond in **4** as a function of ring conformation (Figure 3) is apparently induced by intramolecular H-bonding between O2 and O3, which is not possible in **3**. This rotation induces changes in the C3−H3 bond length by altering the geometric relationship between this bond and the lone-pair orbitals on O3. The "normal" behavior of the C3−H3 bond in **3** and the relatively limited rotation about the C3−O3 bond in **3** relative to that observed in **4** (Figure 3) provide additional evidence of the importance of *vicinal* lone-pair effects on C−H bond lengths in aldofuranosyl rings.

The exocyclic C−O bond lengths in **3** exhibit a dependence on ring conformation similar to that observed in **4** (Figure 4A,B). As observed for C−H bonds, the exocyclic C−O bonds are longer when quasi-axial and shorter when quasi-equatorial; thus, for example, the C1−O1 bond is longer in E_0 than in ^0E (Figure 4A). The C1−O1 bond length appears similar in **3** and **4** (Figure 4A), whereas the C3−O3 bond in **3** is predicted to be shorter than that in **4** for all ring conformations (Figure 4B). This behavior is consistent with recent observations by Gelbin *et al.*[56] based on an analysis of C−O bond lengths in a wide range of nucleosides and nucleotides determined by X-ray crystallography (see Discussion below). The endocyclic C1−O4 and C4−O4 bond lengths in **3** and **4** show similar correlations with ring conformation (Figure 5A,B), although small uniform shifts in these curves are observed ($C1-O4_{deoxyribo} > C1-O4_{ribo}$; $C4-O4_{deoxyribo} < C4-O4_{ribo}$).

The exocyclic C4−C5 bond length in **3** and **4** shows the same dependence on ring conformation (Figure 6). As observed for other exocyclic bonds, this bond is longer when quasi-axial (*e.g.*, ^4E) than when quasi-equatorial (*e.g.*, E_4). The C4−C5 bond length appears essentially unaffected by C2 structure (oxy *vs* deoxy).

C1−O1 bond rotation in **3** as a function of ring conformation appears more restricted than observed in **4**, although the overall pattern is similar in both compounds (Figure 7A). Similar behavior in the C4−O4−C1 bond angle (Figure 7B) and

(55) (a) Wu, G. D.; Serianni, A. S.; Barker, R. *J. Org. Chem.* **1983**, *48*, 1750−1757. (b) Kline, P. C.; Serianni, A. S. *Magn. Reson. Chem.* **1990**, *28*, 324−330. (c) Kline, P. C.; Serianni, A. S. *Magn. Reson. Chem.* **1988**, *26*, 120−123.

(56) Gelbin, A.; Schneider, B.; Clowney, L.; Hsieh, S.-H.; Olson, W. K.; Berman, H. M. *J. Am. Chem. Soc.* **1996**, *118*, 519−529.

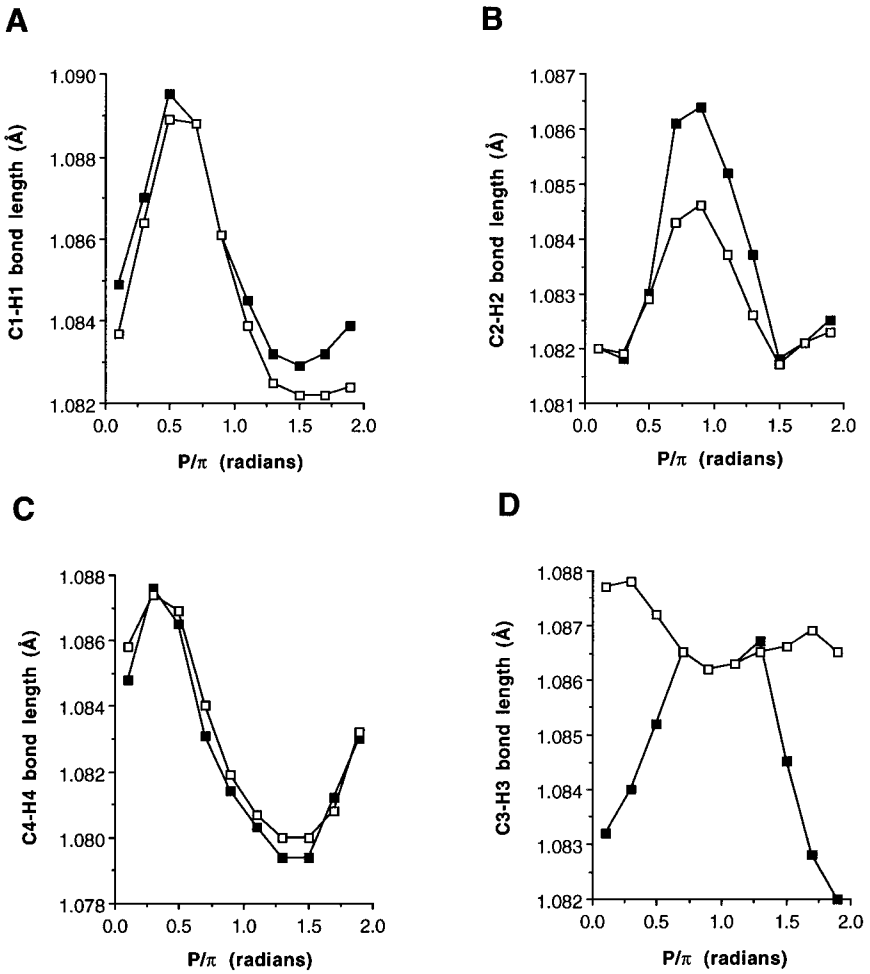

Figure 2. Effect of ring conformation on C1−H1 (A), C2−H2/C2−H2*S* (B), C4−H4 (C), and C3−H3 (D) bond lengths in 2-deoxy-*β*-D-*erythro*-pentofuranose **3** (open squares) and *β*-D-ribofuranose **4** (closed squares) determined from *ab initio* molecular orbital calculations (HF/6-31G*).

puckering amplitude (τ_m) (Figure 7C) in **3** and **4** is also observed, although slightly smaller τ_m values are predicted for **3** in the eastern hemisphere of the itinerary. These latter data indicate that τ_m is not constant throughout the pseudorotational itinerary for **3** and **4**; smaller values are predicted in the western hemisphere, in agreement with molecular dynamics results reported by Harvey and Prabhakaran.[22]

C. Behavior of Computed J_{CH} Values in 3 and Comparisons to Related Couplings in 4. Using computational methods described previously,[27,28,30,31] the *ab initio* molecular orbital data obtained on **3** were used to compute $^1J_{CH}$, $^2J_{CH}$, and $^3J_{CH}$ values in **3** as a function of ring conformation. These couplings are compared to corresponding values reported previously for **4**[28] in order to assess the effect of C2 structure on coupling magnitudes. Having compared the behavior of individual $^{13}C-^1H$ spin-couplings in **3** and **4** derived from computational methods, we then test these results by examining experimentally-determined $^{13}C-^1H$ spin-couplings in the structurally-related methyl glycosides, **5** and **6** (see section E below).

One-Bond $^{13}C-^1H$ Couplings. The dependence of $^1J_{C1,H1}$ magnitude on ring conformation in **3** and **4** is essentially the same (Figure 8A), indicating that the presence or absence of an hydroxyl group at C2 has little effect on $^1J_{C1,H1}$ magnitude. Similar behavior is observed in the methyl pyranosides of D-glucose and 2-deoxy-D-glucose (2-deoxy-D-*arabino*-hexose): $^1J_{C1,H1}$ (α-*gluco* **7**) = 170.1 Hz, $^1J_{C1,H1}$ (2-deoxy-α-*gluco* **8**) = 170.4 Hz, $^1J_{C1,H1}$ (*β*-*gluco* **9**) = 161.3 Hz, and $^1J_{C1,H1}$ (2-deoxy-*β*-*gluco* **10**) = 161.8 Hz. These data indicate that $^1J_{C1,H1}$ values are essentially the same in conformationally defined aldopyranoses and their 2-deoxy analogs, thus providing experimental support for the predicted behavior of $^1J_{C1,H1}$ in **3** and **4** (Figure 8A). In both **3** and **4**, $^1J_{C1,H1}$ is larger for quasi-equatorial or near quasi-equatorial C1−H1 bonds (shorter bond, more *s*-character) and smaller for quasi-axial or near quasi-axial C1−H1 bonds (longer bond, less *s*-character).[27,28]

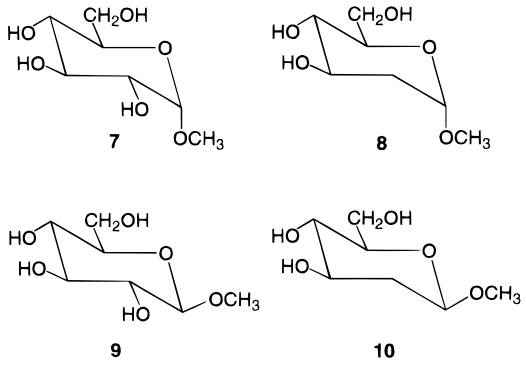

$^1J_{C2,H2S}$ in **3** and $^1J_{C2,H2}$ in **4** show the same dependence on ring conformation (Figure 8B), with larger values predicted when the C2−H2 bond is quasi-equatorial (*e.g.*, E_2) and smaller values predicted when the bond is quasi-axial (*e.g.*, ^2E). In addition, the absence of an oxygen substituent at C2 in **3** causes a large and fairly uniform reduction (∼17 Hz) in coupling magnitude. $^1J_{C3,H3}$ in **3** and **4** exhibits the same general dependence on ring conformation, but $^1J_{C3,H3}$ in **3** is reduced in magnitude by ∼4 Hz relative to $^1J_{C3,H3}$ in **4**.

$^1J_{C4,H4}$ in **3** and **4** are similar in magnitude and exhibit essentially the same dependence on ring conformation (Figure

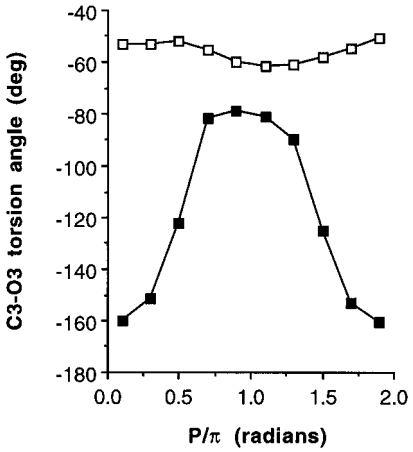

Figure 3. Effect of ring conformation on the C3−O3 torsion angle (defined as H3−C3−O3−H) in **3** (open squares) and **4** (closed squares) determined from *ab initio* molecular orbital calculations (HF/6-31G*).

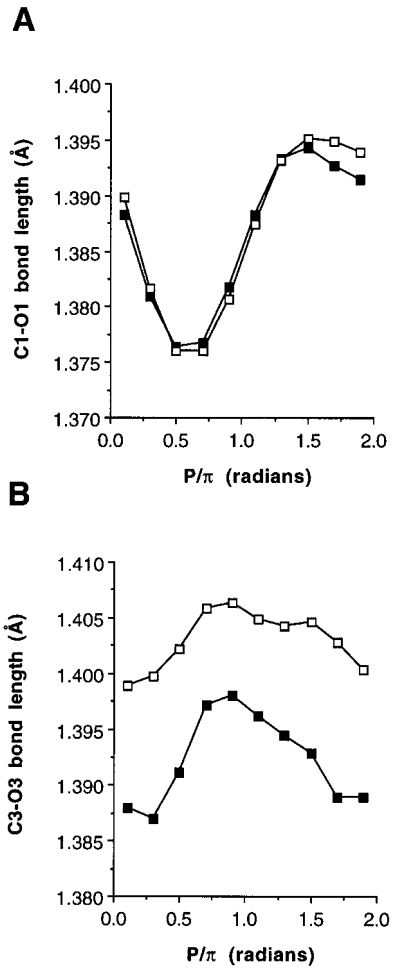

Figure 4. Effect of ring conformation on exocyclic C−O bond lengths in **3** (open squares) and **4** (closed squares) determined from *ab initio* molecular orbital calculations (HF/6-31G*). (A) C1−O1 bond and (B) C3−O3 bond.

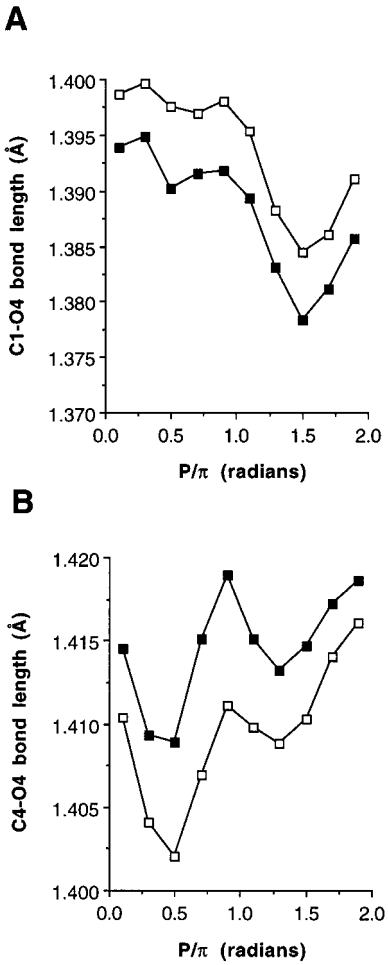

Figure 5. Effect of ring conformation on endocyclic C−O bond lengths in **3** (open squares) and **4** (closed squares) determined from *ab initio* molecular orbital calculations (HF/6-31G*). (A) C1−O4 bond and (B) C4−O4 bond.

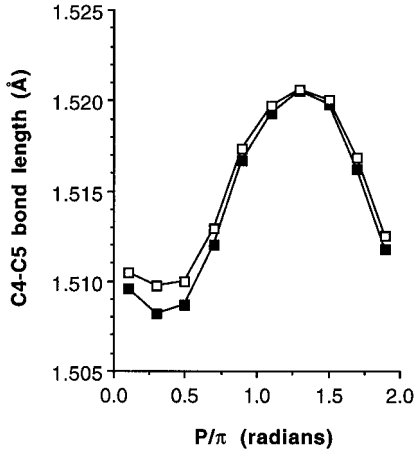

Figure 6. Effect of ring conformation on the exocyclic C4−C5 bond length in **3** (open squares) and **4** (closed squares) determined from *ab initio* molecular orbital calculations (HF/6-31G*).

8D). A shift to slightly smaller values is predicted for conformers of **3** (relative to **4**) lying in the southern hemisphere of the itinerary. As found for other $^1J_{CH}$ in **3** and **4**, $^1J_{C4,H4}$ is larger when the C4−H4 bond is quasi-equatorial (*e.g.*, ^{4}E) and smaller when this bond is quasi-axial (*e.g.*, E_4).

Two-Bond ^{13}C−^{1}H Couplings. $^2J_{C1,H2S}$ in **3** and $^2J_{C1,H2}$ in **4** show a similar dependence on ring conformation, with more negative (less positive) couplings found in S forms than in N forms (Figure 9A). The curve for **3** is shifted to more negative couplings relative to that for **4** (∼ −4−6 Hz), indicating that the loss of an electronegative substituent at the carbon bearing the coupled proton (C−C−H coupling pathway) causes a shift to more *negative* couplings. A similar trend is observed for $^2J_{C3,H2}$, which exhibits the same dependence on ring conformation in **3** and **4** yet is shifted to more *negative* values in **3** (∼ −1 Hz) (Figure 9B). In contrast, $^2J_{C2,H1}$ in **3** and **4** is relatively insensitive to ring conformation, with more *positive* couplings predicted in **3** (Figure 9C). The latter result suggests

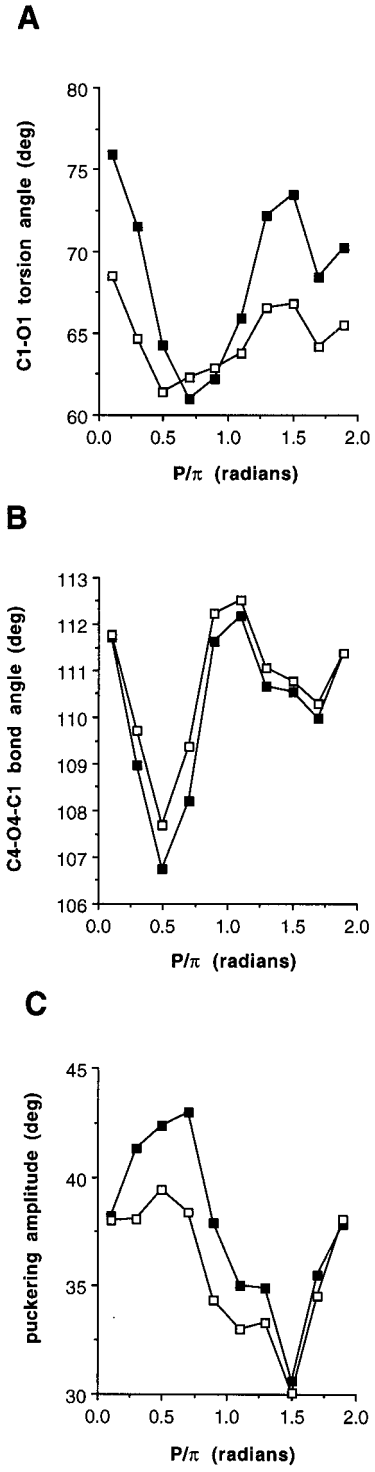

Figure 7. Effect of ring conformation on (A) the C1−O1 torsion angle (defined as H1−C1−O1−H), (B) the C4−O4−C1 bond angle, and (C) puckering amplitude (τ_m) in **3** (open squares) and **4** (closed squares) determined from *ab initio* molecular orbital calculations (HF/6-31G*).

that the loss of an electronegative substituent at the coupled carbon (C−C−H coupling pathway) results in a shift to more *positive* couplings. A similar shift is observed for $^2J_{C2,H3}$, which exhibits the same dependence on ring conformation in **3** and **4** but is displaced to more *positive* values in **3** (Figure 9D).

$^2J_{C3,H4}$ values are similar in magnitude and negative in sign in **3** and **4** and are relatively insensitive to ring conformation (Figure 9E). In contrast, $^2J_{C4,H3}$ exhibits a strong sensitivity to ring conformation in **3** and **4**, with couplings displaced to slightly more negative (less positive) values in **3** (Figure 9F). This latter shift suggests that structural changes at a carbon adjacent to that bearing the coupled proton can affect $^2J_{CCH}$ magnitude. Related "remote" effects on $^2J_{CCH}$ values have been observed previously in aldopyranosyl rings.[57]

Three-Bond ^{13}C−^{1}H Couplings. $^3J_{CH}$ values in carbohydrates exhibit a dihedral angle dependence as expected,[58] although other factors (*e.g.*, α-substituent effects)[59] also influence the magnitudes of these couplings. Six C−C−C−H and two C−O−C−H coupling pathways exist in **3** that are potentially sensitive to ring conformation, and the corresponding C−H torsion angles determined from *ab initio* calculations are shown in Figure 10. Two couplings pathways, namely, C1−C2−C3−H3 and C4−C3−C2−H2*R*, show essentially the same dependence of dihedral angle on ring conformation, and, thus, $^3J_{C1,H3}$ and $^3J_{C4,H2R}$ should exhibit similar overall correlations with ring conformation in 2-deoxy-*β*-D-*ribo* rings.

The response of $^3J_{C1,H3}$ to ring conformation in **3** and **4** is similar (Figure 11A), indicating that structural differences at C2 do not appreciably affect coupling magnitude. This observation is consistent with those made previously[60] in the methyl pyranosides of D-glucose and 2-deoxy-D-glucose: $^3J_{C1,H3}$ (α-*gluco* **7**) = ∼0 Hz, $^3J_{C1,H3}$ (2-deoxy-α-*gluco* **8**) = ∼0 Hz, $^3J_{C1,H3}$ (*β*-*gluco* **9**) = 1.3 Hz, and $^3J_{C1,H3}$ (2-deoxy-*β*-*gluco* **10**) = <0.8 Hz. These latter data suggest similar or smaller $^3J_{C1,H3}$ values upon deoxygenation at the central carbon of a C−C−C−H coupling pathway, at least for C−C−C−H dihedral angles of ∼60°.

$^3J_{C1,H4}$ values show a similar dependence on ring conformation in **3** and **4** (Figure 11B). As observed for $^3J_{C1,H3}$ (Figure 11A), small differences are observed at the larger dihedral angles, with **3** exhibiting slightly larger couplings; this latter result (which is also observed in other $^3J_{CH}$ as discussed below) cannot be attributed to differences in C−C−C−H dihedral angle, since ring puckering in **3** is less than or approximately equal to that in **4** (Figure 7C). Like $^3J_{C1,H4}$, $^3J_{C4,H1}$ values are very similar in **3** and **4** and show essentially the same correlation with ring conformation (Figure 11C). The overall change in coupling magnitude observed for $^3J_{C1,H4}$ and $^3J_{C4,H1}$ (∼0−8 Hz) is larger than that observed for $^3J_{C1,H3}$ (∼0−6 Hz) (Figure 11A), which is consistent with previous experimental observations made in aldopyranosides;[57] the presence of a heteroatom in the C−O−C−H coupling pathway generally increases coupling magnitude relative to a C−C−C−H pathway involving the same dihedral angle.

Notable differences are observed in the response of $^3J_{C2,H4}$ to ring conformation in **3** and **4** (Figure 11D). In contrast to the behavior of $^3J_{C1,H3}$, $^3J_{C1,H4}$ and $^3J_{C4,H1}$, the overall change in coupling magnitude for $^3J_{C2,H4}$ is small (<4 Hz). Moreover, the dependence on ring conformation is biphasic, that is, two discrete maxima and minima are observed along the pseudorotational itinerary. For **3**, these minima and maxima have similar values, whereas for **4** the maxima differ. In the latter case, the "enhanced" coupling may be attributed to α-substituent effects[59] caused when O2 lies in the C2−C3−C4−H4 plane. Given the biphasic nature of the curves in Figure 11D, the

(57) Podlasek, C. A.; Wu, J.; Stripe, W. A.; Bondo, P. B.; Serianni, A. S. *J. Am. Chem. Soc.* **1995**, *117*, 8635−8644.

(58) (a) Schwarcz, J. A.; Perlin, A. S. *Can. J. Chem.* **1972**, *50*, 3667−3676. (b) Spoormaker, T.; de Bie, M. J. A. *Recl. Trav. Chim. Pays-Bas.* **1978**, *97*, 85. (c) Tvaroska, I.; Gajdos, J. *Carbohydr. Res.* **1995**, *271*, 151−162. (d) Mulloy, B.; Frenkiel, T. A.; Davies, D. B. *Carbohydr. Res.* **1988**, *184*, 39. (e) Tvaroska, I.; Hricovini, H.; Petrakova, E. *Carbohydr. Res.* **1989**, *189*, 359.

(59) van Beuzekom, A. A.; de Leeuw, F. A. A. M.; Altona, C. *Magn. Reson. Chem.* **1990**, *28*, 68−74.

(60) Bandyopadhyay, T.; Wu, J.; Serianni, A. S. *J. Org. Chem.* **1993**, *58*, 5513−5517.

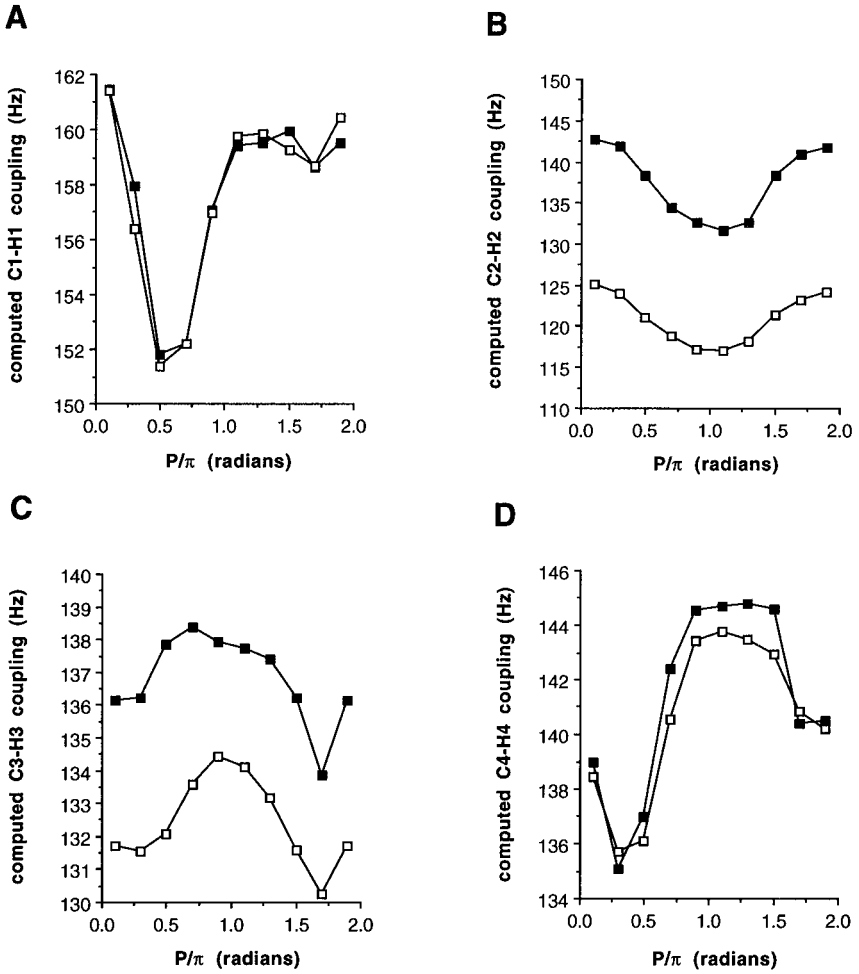

Figure 8. Computed $^1J_{CH}$ values in **3** (open squares) and **4** (closed squares) as a function of ring conformation: (A) $^1J_{C1,H1}$, (B) $^1J_{C2,H2}/^1J_{C2,H2S}$, (C) $^1J_{C3,H3}$, and (D) $^1J_{C4,H4}$.

interpretation of $^3J_{C2,H4}$ in **3** and **4** in conformational terms is likely to be complicated, as discussed previously.[61]

The response of $^3J_{C3,H1}$ to ring conformation in **3** and **4** is similar (Figure 11E) and, as observed for $^3J_{C1,H3}$ and $^3J_{C1,H4}$, couplings in **3** are slightly larger than those observed in **4** at the larger dihedral angles. These results suggest that structure at the intervening C2 carbon affects coupling magnitude. Interestingly, $^3J_{C3,H1}$ in methyl α-D-glucopyranoside is 0.6 Hz larger than $^3J_{C3,H1}$ in methyl α-D-mannopyranoside despite similar C3−C2−C1−H1 dihedral angles (∼180°),[57] again suggesting that structure at C2 influences the coupling. The overall change in coupling for $^3J_{C3,H1}$ in **3** and **4** is smaller (<4 Hz) than observed for $^3J_{C1,H3}$ (<6 Hz) (Figure 11A), which is consistent with observations made previously on related coupling pathways in aldopyranosyl rings.[57]

$^3J_{C4,H2}$ values exhibit the same dependence on ring conformation in **3** and **4** (Figure 11F). The overall change in coupling magnitude is considerably greater (<7 Hz), and the pattern is less complex than observed for the reverse pathway (*i.e.*, C2−C3−C4−H4) for both **3** and **4** (Figure 11D). The similar behavior of $^3J_{C4,H2}$ in **4** and $^3J_{C4,H2S}$ in **3** suggests that the loss of an electronegative substituent at C2 (*i.e.*, the carbon bearing the coupled proton) does not affect coupling magnitude significantly, although some differences are observed at the larger dihedral angles.

D. Internuclear ^{1}H−^{1}H Distances in 3. Previous studies have shown[28,62] that only one ^{1}H−^{1}H internuclear distance is sensitive to ring conformation in **4**, namely, r_{H1-H4}. In **3**, two distances change substantially with ring conformation, namely, r_{H1-H4} and r_{H2R-H4} (Figure 12A). The remaining ^{1}H−^{1}H distances in **3** that do not involve H5*R* and H5*S* are relatively insensitive to ring conformation (Figure 12B,C). Data in Figure 12 are in general agreement with those reported previously by Wüthrich.[62]

The H1−H4 and H2*R*−H4 distances in **3** respond differently to ring conformation (Figure 12A). Thus, for example, in a conventional N/S exchange process (*e.g.*, ^{3}E/^{2}E), r_{H1-H4} remains relatively constant at ∼3.3 Å in both forms; in contrast, for a similar exchange process, r_{H2R-H4} changes from ∼2.7 Å in ^{3}E to ∼4.0 Å in ^{2}E. It is well-known that conformational exchange causes nonlinear averaging of ^{1}H−^{1}H distances derived from NOE or relaxation measurements.[23] Thus, for a simple ^{3}E/^{2}E exchange pathway, r_{H1-H4} values derived experimentally will be ∼3.3 Å regardless of the proportion of N and S forms in solution. More importantly, however, r_{H2R-H4} values will be skewed in favor of the lower distance (∼2.7 Å) unless S forms are very highly favored (*i.e.*, > ∼95%) in solution. For proportions of S forms <∼95%, r_{H2R-H4} values derived experimentally will approach ∼2.7 Å due to the r^{-6} dependence of the NOE and relaxation rates. Consequently, appropriate caution must be exercised when interpreting ^{1}H−^{1}H internuclear distances in **3** in terms of N/S conformational equilibria, even when these distances are sensitive to changes in ring conformation.

(61) Bandyopadhyay, T.; Wu, J.; Stripe, W. A.; Carmichael, I.; Serianni, A. S. *J. Am. Chem. Soc.* **1997**, *119*, 1737−1744.

(62) Wüthrich, K. *NMR of Proteins and Nucleic Acids* J. Wiley and Sons: New York, 1986.

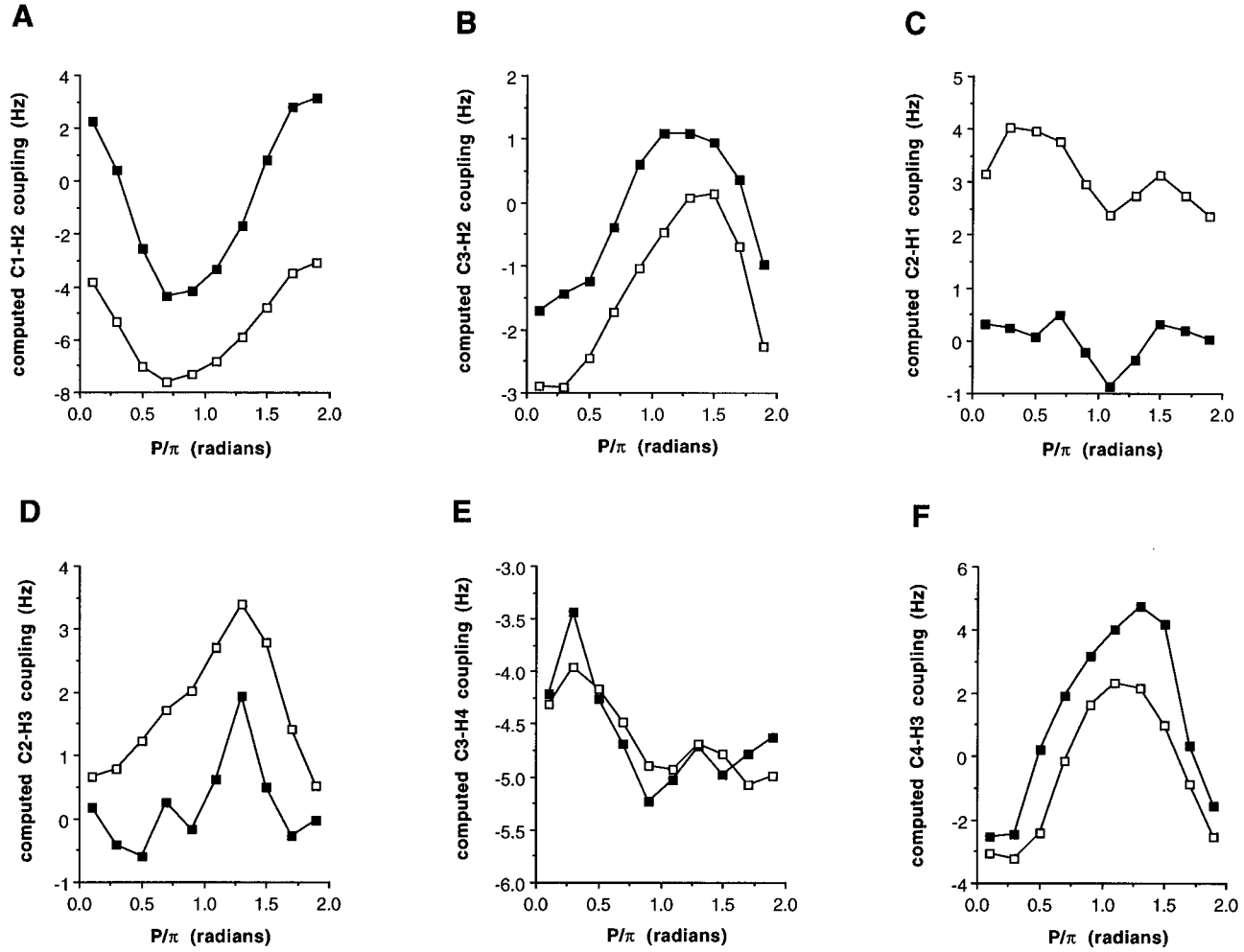

Figure 9. Computed $^2J_{CH}$ values in **3** (open squares) and **4** (closed squares) as a function of ring conformation: (A) $^2J_{C1,H2}/^2J_{C1,H2S}$, (B) $^2J_{C3,H2}/^2J_{C3,H2S}$, (C) $^2J_{C2,H1}$, (D) $^2J_{C2,H3}$, (E) $^2J_{C3,H4}$, and (F) $^2J_{C4,H3}$.

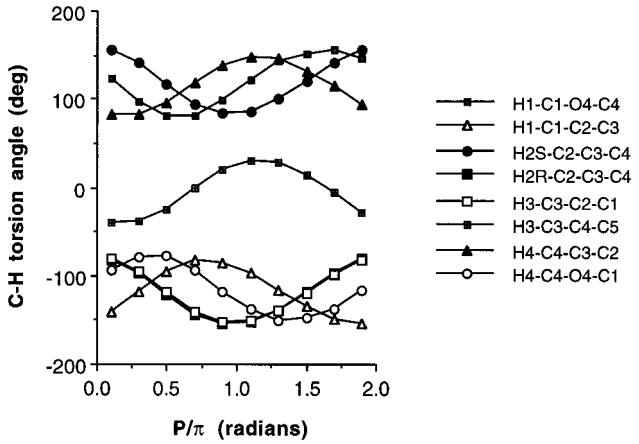

Figure 10. Effect of ring conformation on the eight C−H torsion angles in **3** determined from *ab initio* molecular orbital calculations (HF/6-31G*). Only those torsions sensitive to ring conformation are shown.

E. Analysis of J_{CH} and J_{CC} Values in Methyl β-D-Ribofuranoside 5 and Methyl 2-Deoxy-β-D-ribofuranoside 6. $^{13}C-^1H$ and $^{13}C-^{13}C$ spin-coupling constants (one-, two-, and three-bond) observed in **5** and **6** in ^2H_2O solvent are given in Table 4. In the following discussion, these couplings are examined as potential probes to assign ^1H chemical shifts of diastereotopic protons and to assess hydroxymethyl group and ring conformations in **5** and **6**.

Assignment of the Diastereotopic C2 and C5 Protons, and Hydroxymethyl Conformation. As shown recently in 2′-deoxyribonucleosides,[60] $^2J_{C1,H2R}$ and $^2J_{C1,H2S}$ values in 2-deoxy-β-D-ribofuranosyl rings **2** can differ substantially (*e.g.*, $^2J_{C1',H2'S} = -5.7$ Hz and $^2J_{C1',H2'R} = \pm 0.4$ Hz in 2′-deoxyadenosine).[60] Using deoxypyranose model compounds, it was demonstrated that large *negative* couplings are possible only for $^2J_{C1',H2'S}$, while $^2J_{C1',H2'R}$ is considerably smaller in absolute value. Data in Figure 13A confirm this behavior in **3**. This difference can be exploited to assign the H2*R* and H2*S* signals in the ^1H NMR spectrum of **6**. In **6**, the less shielded C2 proton exhibits a coupling of −4.6 Hz, and the more shielded a coupling of −1.5 Hz. Thus, the more-shielded C2 proton may be assigned to H2*R* (Table 1).

Assignment of the H5*R* and H5*S* signals of **5** and **6** can be made using $^3J_{HH}$ values ($^3J_{H4,H5R}$, $^3J_{H4,H5S}$) in conjunction with $^2J_{CH}$ ($^2J_{C4,H5R}$, $^2J_{C4,H5S}$) or $^3J_{CH}$ ($^3J_{C3,H5R}$, $^3J_{C3,H5S}$) values, as illustrated previously in the assignment of the prochiral C4 proton signals of tetrofuranoses and their derivatives.[26a] These couplings can be predicted in the three staggered C4−C5 bond rotamers (*gg*, *gt*, *tg*) (Chart 5) using appropriate Karplus equations for $^3J_{HH}$[48] and $^3J_{CH}$[58a−c] and empirical rules for predicting the magnitudes and signs of $^2J_{CH}$ values.[58a,63,64] Correlations between coupling magnitude and sign, and C4−C5 rotamer, for various *J* values are given in Table 5. In contrast to other couplings found in Table 5, $^2J_{C5,H4}$ values cannot be used to assign the H5*R* and H5*S* signals but are useful

(63) Schwarcz, J. A.; Cyr, N.; Perlin, A. S. *Can. J. Chem.* **1975**, *53*, 1872.
(64) Bock, K.; Pedersen, C. *Acta Chem. Scand. Ser. B* **1977**, *31*, 354.

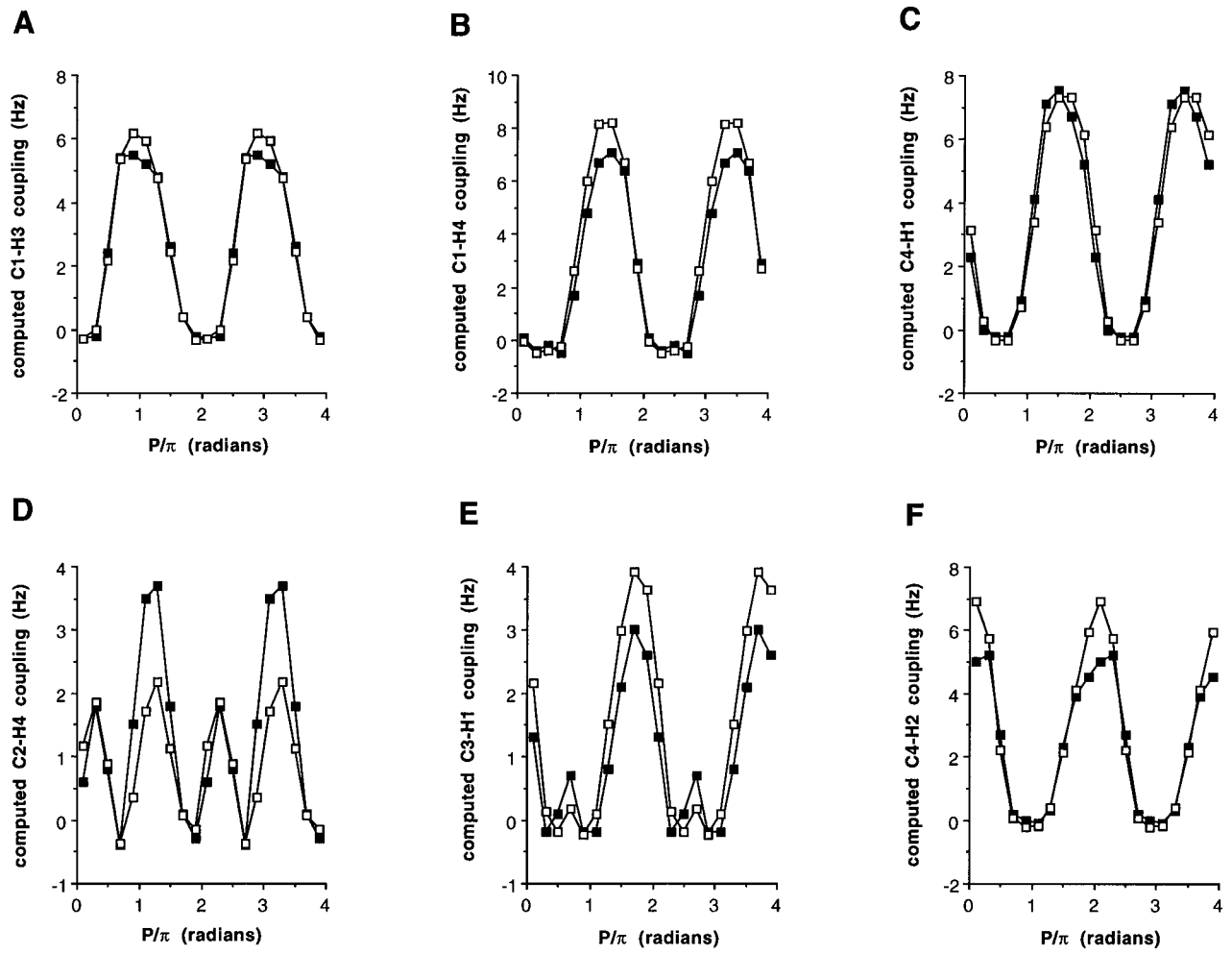

Figure 11. Computed $^3J_{CH}$ values in **3** (open squares) and **4** (closed squares) as a function of ring conformation: (A) $^3J_{C1,H3}$, (B) $^3J_{C1,H4}$, (C) $^3J_{C4,H1}$, (D) $^3J_{C2,H4}$, (E) $^3J_{C3,H1}$, and (F) $^3J_{C4,H2}/^3J_{C4,H2S}$.

in assessing the relative populations of the three rotamers, as discussed below.

Data in Table 5 can be used qualitatively to assign the H5*R* and H5*S* signals in **5**. The more shielded C5 proton (defined as H5′) exhibits a larger coupling to H4 (6.6 Hz) than the less shielded C5 proton (defined as H5; 3.1 Hz) (Table 1). Thus, H5′ experiences a *trans* relationship with H4 more frequently than does H5, and two arrangements about the C4−C5 bond are consistent with these data, one in which H5*R* is antiperiplanar to H4 (rotamer A, Chart 5) and one in which H5*S* is antiperiplanar to H4 (rotamer B, Chart 5). The two possibilities are distinguished by noting that C3 exhibits similar couplings to H5 and H5′ in **5** (∼3.0 and 2.1 Hz, respectively) (Table 4). These data are more consistent with rotamer A than with rotamer B (Chart 5), since C3 is *gauche* to both H5 and H5′ in the former. Therefore, the more shielded C5 proton (H5′) can be assigned as H5*R*; this conclusion is consistent with H5*R*/H5*S* signal assignments based on selective deuteration.[55a] A similar treatment of corresponding coupling data in **6** leads to the same conclusion (*i.e.*, the more shielded C5 proton is H5*R*) (Table 1).

The above approach is not limited to $^3J_{H4,H5R}$ and $^3J_{H4,H5S}$ values that differ in magnitude, such as observed in **5** and **6** (Table 1). For example, in methyl α-D-ribofuranoside **11**, $^3J_{H4,H5}$ = 3.3 Hz and $^3J_{H4,H5'}$ = 4.6 Hz.[43] One C4−C5 rotamer is consistent with these data in which H4 is *gauche* to both H5*R* and H5*S* (rotamer C, Chart 5). The stereochemical assignments can be made by noting that $^3J_{C3,H5}$ = 4.3 Hz and $^3J_{C3,H5'}$ = 2.2 Hz; thus H5 = H5*S* and H5′ = H5*R*, in accord with assignments based on selective deuteration.[55a]

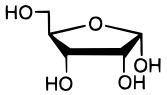

11

An alternative method to assign the H5*R* and H5*S* signals involves the concerted use of $^3J_{HH}$ and $^2J_{CH}$ values. Thus, for **5**, rotamers A and B in Chart 5 can be distinguished by noting that $^2J_{C4,H5R}$ will be small and negative while $^2J_{C4,H5S}$ will be large and positive in rotamer A (*gt*), while both $^2J_{CH}$ values will be small and negative in rotamer B (*tg*) (Table 5). In both **5** and **6**, a relatively large difference is observed between these $^2J_{CH}$ values (Δ = ∼1.8 and ∼3.4 Hz, respectively) (Table 4), with the less shielded C5 proton (H5) exhibiting the more positive (less negative) coupling. These data are consistent with rotamer A (Chart 5) and permit an assignment of the more shielded C5 proton to H5*R* in both compounds.

Assignment of the H5*R* and H5*S* signals in **5** and **6** allows an estimation of C4−C5 rotamer populations based on $^3J_{HH}$ values (Table 3). $^2J_{C5,H4}$ values in **5** and **6** are consistent with populations determined from the magnitudes of $^3J_{H4,H5R}$ and $^3J_{H4,H5S}$.[55b] Conversion of **5** to **6** results in essentially no change in P_{gt} but a substantial increase in P_{tg} and decrease in P_{gg} (Table 3). This change in populations should induce a shift to a less positive (more negative) value for $^2J_{C5,H4}$, as observed ($^2J_{C5,H4}$ = −0.9 Hz in **5** and $^2J_{C5,H4}$ = −1.7 Hz in **6**).

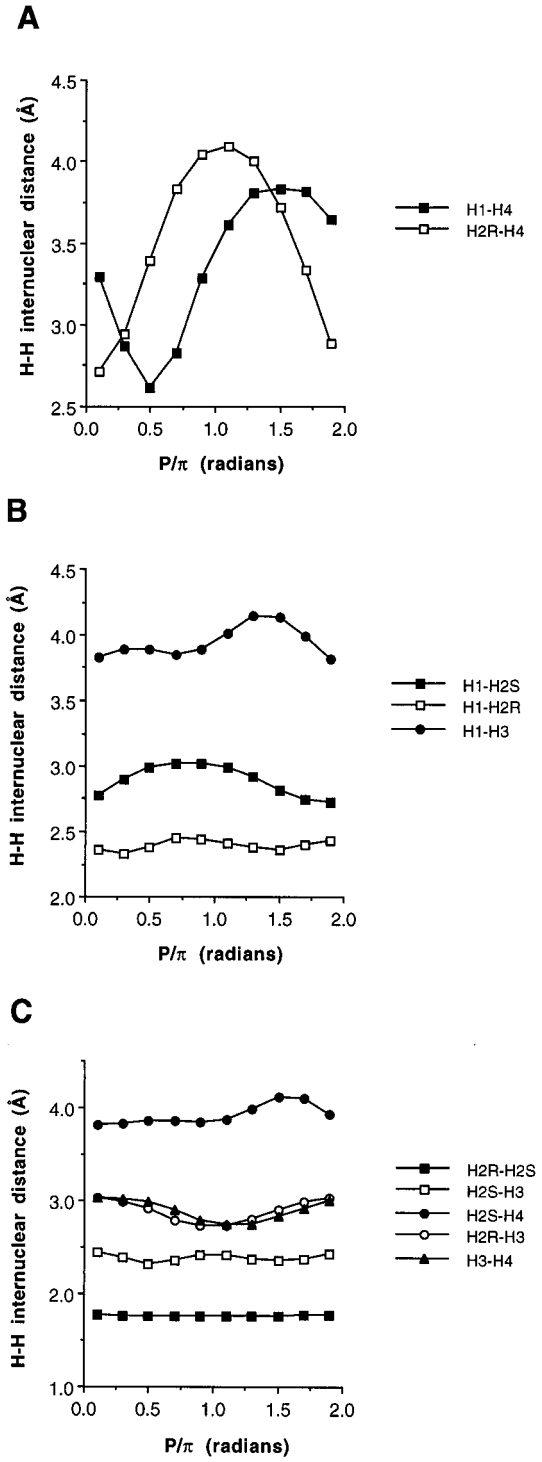

Figure 12. Effect of ring conformation on internuclear $^1H-^1H$ distances in **3** determined from *ab initio* molecular orbital calculations (HF/6-31G*).

In oligonucleotides, conformation about the C4′−C5′ bond is relatively constrained, thus leading to observed $^3J_{H4',H5'R/S}$, $^2J_{C4',H5'R/S}$, and $^2J_{C5',H4'}$ values that are consistent with a single rotamer. Thus, as shown by Griesinger and co-workers,[65] residues in RNA oligomers in which the *gg* conformation about the C4′−C5′ bond is preferred (rotamer C, Chart 5) yield $^2J_{C4',H5'R}$ and $^2J_{C4',H5'S}$ values similar to those predicted by empirical methods (±1.5 Hz and −4.4 ±1.0 Hz, respectively), thus making H5*R* and H5*S* assignments more straightforward.[19,65]

(65) Marino, J. P.; Schwalbe, H.; Glaser, S. J.; Griesinger, C. *J. Am. Chem. Soc.* **1996**, *118*, 4388−4395.

Table 3. C4−C5 Bond Rotamer Populations[a] for Methyl β-D-ribofuranoside **5** and Methyl 2-Deoxy-β-D-ribofuranoside **6** Based on $^3J_{HH}$ Data[b]

rotamer[c]	**5**	**6**
gg, +*sc*	0.38 (0.04)	0.21 (0.02)
gt, *ap*	0.52 (0.04)	0.52 (0.03)
tg, −*sc*	0.10 (0.02)	0.26 (0.01)

[a] Data taken from ref 55b; in ^2H_2O solvent, ~25 °C; values in parentheses are standard deviations. [b] $^3J_{H4,H5R}$ and $^3J_{H4,H5S}$ data provided in Table 1. [c] Rotamers shown in Chart 5.

Table 4. $^{13}C-^1H$ and $^{13}C-^{13}C$ Spin-Couplings[a] in Methyl β-D-ribofuranoside **5** and Methyl 2-Deoxy-β-D-ribofuranoside **6**

compound **5**		compound **6**	
coupled nuclei	*J* (Hz)	coupled nuclei	*J* (Hz)
C1−H1	174.3	C1−H1	173.9
C1−H2	0	C1−H2*R*	−1.5
C1−H3	1.2	C1−H2*S*	−4.6
C1−H4	2.9	C1−H3	2.7
C1−O*CH*$_3$	4.3	C1−H4	4.8
C2−H1	~ −0.8	C1−O*CH*$_3$	4.5
C2−H2	154.6	C2−H1	2.1
C2−H3	+1.2	C2−H2*R*	132.2
C2−H4	0.9	C2−H2*S*	134.0
C3−H1	3.1	C2−H3	0 (br)
C3−H2	−0.7	C2−H4	~1.2
C3−H3	148.0	C3−H1	3.3
C3−H4	~ −5.5	C3−H2*R*	−6.4
C3−H5*R*	2.1	C3−H2*S*	−2.1
C3−H5*S*	~ 3.0	C3−H3	149.5
C4−H1	4.5	C3−H4	~ −5.5
C4−H2	~ 4.3	C3−H5*R*	2.9
C4−H3	−0.7	C3−H5*S*	2.7
C4−H4	148.1	C4−H1	5.0
C4−H5*R*	~ −2.7	C4−H2*R*	2.0
C4−H5*S*	−0.9	C4−H2*S*	4.2
C5−H3	~ 4.8	C4−H3	1.5[b]
C5−H4	−0.9	C4−H4	149.0
C5−H5*R*	143.5	C4−H5*R*	−3.4
C5−H5*S*	142.4	C4−H5*S*	0
		C5−H3	4.0
C1−C2	46.8	C5−H4	−1.7
C1−C3	3.0	C5−H5*R*	143.8
C1−C4	0	C5−H5*S*	142.2
C1−C5	br		
C1−O*CH*$_3$	2.0	C1−C2	40.5
C2−C3	37.2	C1−C3	br
C2−C4	1.0	C1−C4	0
C2−C5	1.8	C1−C5	0
C2−O*CH*$_3$	3.5	C1−O*CH*$_3$	1.8
C3−C4	39.2	C2−C3	35.4
C3−C5	2.3	C2−C4	1.4
C4−C5	42.0	C2−C5	1.1
		C2−O*CH*$_3$	3.0
		C3−C4	37.9
		C3−C5	3.6
		C4−C5	41.5

[a] ~30 °C, ±0.1 Hz unless otherwise indicated. [b] Sign uncertain.

Ring Conformation. One-Bond $^{13}C-^1H$ Couplings. $^1J_{C1,H1}$ in **5** and **6** are 174.3 and 173.9 Hz, respectively. These couplings are predicted to be similar due to the effects of conformational averaging. Using the two-state models for **5** and **6** based on an analysis of $^3J_{HH}$ values (Table 2) and data in Figure 8A (*ribo*: 159.5 Hz in E_2, 157.1 Hz in ^2E; deoxy*ribo*: 160.4 Hz in E_2, 159.8 Hz in E_3), couplings of 159.4 and 160.2 Hz are calculated for $^1J_{C1,H1}$ in **5** and **6**, respectively. While not accurate in absolute terms, the approximately similar computed values for $^1J_{C1,H1}$ in **5** and **6** are consistent with the experimental data.

$^1J_{C2,H2}$ and $^1J_{C3,H3}$ values in **5** are substantially different (154.6 and 148.0 Hz, respectively) (Table 4). This difference is caused

Table 5. Predicted[a] Coupling Magnitudes and Signs in C4−C5 Bond Rotamers of **5** and **6** in Chart 5

coupled nuclei	C4−C5 rotamer		
	gg	*gt*	*tg*
C3,H5*R*	+, small	+, small	+, large
C3,H5*S*	+, large	+, small	+, small
C4,H5*R*	+, large	−, small	−, small
C4,H5*S*	−, small	+, large	−, small
C5,H4	+, large	−, small	−, small
H4,H5*R*	+, small	+, large	+, small
H4,H5*S*	+, small	+, small	+, large

[a] For J_{CH} values: small = 0−2 Hz; large = 4−6 Hz. Magnitudes approximated from $^3J_{CCCH\ (gauche)}$ and $^3J_{CCCH\ (trans)}$ values observed in aldopyranosyl rings;[57] magnitudes and signs of $^2J_{CH}$ values approximated by the projection rule.[64] For J_{HH} values: small = 1−2 Hz; large = 8−10 Hz; predicted from the modified Karplus equation described by Haasnoot *et al.*[48]

by at least two factors: differences in the C2−H2 and C3−H3 bond lengths (which have not been addressed experimentally at the present time) and different average orientations of the C2−H2 and C3−H3 bonds. Since **5** highly prefers the E_2 conformation (Table 2), the latter average orientations are quasi-equatorial and quasi-axial, respectively. Thus, the larger value of $^1J_{C2,H2}$ relative to $^1J_{C3,H3}$ may be expected based on differences in C−H bond orientation, since $^1J_{CH}$ values for a given C−H bond are enhanced when the bond is quasi-equatorial.[27] In addition, the values of $^1J_{C2,H2}$ and $^1J_{C3,H3}$ in **5** are similar in magnitude to $^1J_{C2',H2'}$ (159 ± 2 Hz) and $^1J_{C3',H3'}$ (145 ± 3 Hz) values observed in RNA oligomers for residues in the ^{3}E (N) conformation,[66] thus providing additional evidence of a preferred N conformation for **5**. In contrast, $^1J_{C2',H2'}$ in ribonucleosides is 151.7 ± 1.6 Hz,[43] which is smaller than $^1J_{C2,H2}$ in **5**. The latter difference is attributed to the higher percentage of S forms in aqueous solutions of ribonucleosides; in S forms (*e.g.*, ^{2}E), the C2−H2 bond is quasi-axial or near quasi-axial, resulting in a smaller value for $^1J_{C2,H2}$ than expected in N forms in which this bond is quasi-equatorial or near quasi-equatorial.

$^1J_{C2,H2R}$ and $^1J_{C2,H2S}$ assume different values in **6** (132.2 and 134.0 Hz, respectively) (Table 4). These couplings are expected to exhibit complementary dependencies on ring conformation (Figure 13B), in concert with changes in C−H bond orientation/length. In E_2, $^1J_{C2,H2S} > {}^1J_{C2,H2R}$ (124.1 and 119.0 Hz), whereas the opposite is predicted in E_3 (117.0 and 122.1 Hz) (Figure 13B). The observed relative magnitudes of the observed couplings are consistent with a slight excess population of N forms in solution.

$^1J_{C4,H4}$ values in **5** and **6** are 148.1 and 149.0 Hz, respectively. An inspection of the predicted dependence of $^1J_{C4,H4}$ on ring conformation (Figure 8D) and considerations of the N/S models for **5** and **6** derived from $^3J_{HH}$ analysis (Table 2) indicate that $^1J_{C4,H4}$ should be slightly larger in **6** than in **5** (computed values of 140.7 and 141.6 Hz, respectively), in accord with experimental observations.

$^1J_{C5,H5R}$ (143.7 ± 0.2 Hz) is slightly larger than $^1J_{C5,H5S}$ (142.3 ± 0.1 Hz) in **5** and **6**, but this small difference cannot be interpreted in structural terms at the present time.

Two-Bond ^{13}C−^{1}H Couplings. $^2J_{C1,H2}$ is ∼0 Hz in **5**, whereas the corresponding $^2J_{C1,H2S}$ in **6** is −4.6 Hz (Table 4). The projection rule[64] predicts values of ∼ +2.5 Hz and ∼ −5 Hz for N (E_2) and S (^{2}E) forms of **5**, respectively, whereas corresponding values of ∼0 Hz and ∼ −8 Hz are predicted for **6**. These predictions are consistent with data in Figure 9A for the β-D-*ribo* ring but differ from computed values for N forms of the 2-deoxy-β-D-*ribo* ring. Interestingly, $^2J_{C1,H2R}$ in 2-deoxy-α-D-[1-^{13}C]glucopyranose is −3.8 Hz,[60] although the projection rule predicts a value of ∼0 Hz; this situation is similar to that for $^2J_{C1,H2S}$ in N forms of **6**. In contrast, $^2J_{C1,H2S}$ in 2-deoxy-β-D-[1-^{13}C]glucopyranose is −8.3 Hz,[60] in good agreement with the projection rule prediction of ∼ −8 Hz; this situation is similar to that for $^2J_{C1,H2S}$ in S forms of **6**. Thus, the experimental data in these model compounds support the computed behavior of $^2J_{C1,H2S}$ in Figure 9A and suggest that the projection rule may not be completely reliable when applied to couplings involving the C2 protons of **6**. Nevertheless, the more negative coupling observed in **6** is in qualitative agreement with the predictions when N/S populations are taken into account (Table 2). $^2J_{C1,H2}$ is −2.4 Hz in methyl β-D-erythrofuranoside **12**[26a] and −1.7 to −3.2 Hz in ribonucleosides[43] where N and S forms are present is comparable proportions, whereas $^2J_{C1',H2'}$ is −4.1 Hz in erythroadenosine **13** which highly prefers S forms.[28,67] In RNA oligomers, residues preferring S forms yield $^2J_{C1',H2'}$ values of −3 to −5 Hz.[19] Thus, the small coupling

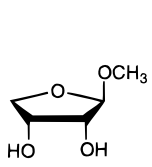

12

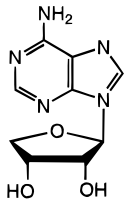

13

observed in **5** is consistent with a preferred N conformation. In 2′-deoxyribonucleosides, $^2J_{C1,H2'S} = \sim -5.7$ Hz;[60] this larger value relative to that observed in **6** results from differences in the preferred N and S forms, differences in N/S populations, and/or substituent effects (at C1). Similar factors are probably responsible for differences in $^2J_{C1,H2R}$, which is −1.5 Hz in **6** and <0.4 Hz in 2′-deoxyribonucleosides.[60]

The difference between $^2J_{C1,H2R}$ and $^2J_{C1,H2S}$ in **6** (Δ = 3.1 Hz) can be used to evaluate N/S equilibrium, as suggested previously.[60] As shown in Figure 13A, $^2J_{C1,H2S}$ becomes more negative (less positive) in the conversion of N to S forms, whereas the opposite is observed for $^2J_{C1,H2R}$. Thus, the *difference* between these couplings should be large in S forms (∼7 Hz) and minimal in N forms (<1 Hz). The observed difference in **6** (3.1 Hz) indicates relatively equal proportions of N and S forms, which is consistent with the $E_2/^4T_3$ conformational model based on $^3J_{HH}$ analysis (Table 2). The difference between $^2J_{C1',H2'R}$ and $^2J_{C1',H2'S}$ is larger in 2′-deoxyribonucleosides (∼5−6 Hz)[60] than in **6**, which reflects differences in N/S populations and/or the preferred N and S forms.

$^2J_{C2,H1}$ is ∼ −0.8 Hz in **5** and +2.1 Hz in **6**, that is, more positive in the deoxyfuranose. Data in Figure 9C indicate that this coupling is relatively insensitive to ring conformation in both compounds. $^2J_{C2,H1}$ is also predicted to be consistently more positive in **6** than in **5** (Figure 9C), in agreement with the observed couplings and with predictions based on the projection rule[64] (∼0 Hz for **5** and ∼ +2.5 Hz for **6** in both E_2 and ^{2}E forms). The difference in the observed couplings (∼3.0 Hz) is similar to the average difference between the computed couplings (∼3.1 Hz, Figure 9C). In contrast, $^2J_{C2',H1'} = -3.3 \pm 0.2$ Hz in ribonucleosides,[43] −2 to −4 Hz in residues of RNA oligomers preferring N forms,[19] and ∼0 Hz in 2′-deoxyribonucleslides,[61] that is, about 2.5 Hz more negative than corresponding values in **5** and **6**. This shift has been attributed primarily to substitution effects at C1 (N vs O) rather than to conformational factors, as discussed in a recent investigation.[61]

$^2J_{C2,H3}$ in **5** and **6** are +1.2 and ∼0 Hz, respectively. In ribonucleosides[43] and 2′-deoxyribonucleosides,[61] $^2J_{C2',H3'}$ is small (absolute value <0.8 Hz), and values of +2−3 Hz and −1.9 to

−2.4 Hz have been observed in RNA oligomers for residues preferring N and S forms, respectively.[19] Application of the projection rule[64] predicts that $^2J_{C2,H3}$ should be ∼0 Hz in N (E_2) and S (^2E) forms of 2′-deoxyribonucleosides, whereas values of ∼ +3 Hz and ∼ −2 Hz are predicted for N and S forms of ribonucleosides, respectively. These predictions for the *β*-D-*ribo* ring differ from computed behavior (Figure 9D), as noted previously,[28] and the discrepancy may be due to effects caused by the large rotation about the C3−O3 bond that occurs during geometry optimization (Figure 3). $^2J_{C2,H3}$ is predicted to become slightly more positive in the 2-deoxy-*β*-D-*ribo* ring as N forms convert to S forms (Figure 9D), which differs from projection rule predictions. These results, especially those for the *β*-D-*ribo* ring, indicate that further study of $^2J_{C2,H3}$ behavior is needed.

$^2J_{C3,H2}$ in **5** is −0.7 Hz, whereas the related $^2J_{C3,H2S}$ in **6** is −2.1 Hz. Data in Figure 9B indicate that this coupling should become more positive (less negative) in the conversion of N to S forms in both compounds and are consistent with predictions for the *β*-D-*ribo* and 2-deoxy-*β*-D-*ribo* rings based on the projection rule[64] (*ribo*: − ∼2.5 Hz in E_2, + ∼3 Hz in ^2E; deoxy*ribo*: − ∼5 Hz in E_2, + ∼2 Hz in ^2E). This coupling is more negative (less positive) in **3** than in **4** for any given ring form (Figure 9B); a similar shift is predicted by the projection rule.[64] Considerations of N/S populations (Table 2) show that $^2J_{C3,H2S}$ in **6** should be ∼1 Hz more negative than $^2J_{C3,H2}$ in **5**, in good agreement with the experimental data. The −0.7 Hz coupling in **5** is less negative than those observed in RNA oligomers for residues preferring N conformations (−0.9 to −1.7 Hz),[19] and this difference may be due, in part, to variations in the preferred N forms. In RNA oligomers, N conformers near ^3E appear more probable than those near E_2, whereas the latter are preferred by **5**; coupling in ^3E is slightly more negative than that in E_2 (Figure 9B).

$^2J_{C3,H2R}$ and $^2J_{C3,H2S}$ are considerably different in **6** (−6.4 and −2.1 Hz, respectively). These couplings are predicted to be negative in sign in nearly all ring conformations (Figure 13C), with $^2J_{C3,H2R}$ more negative than $^2J_{C3,H2S}$ in each ring form, in agreement with experimental observations. The difference in the observed couplings (4.3 Hz) is consistent with a computed difference of 4.5 Hz (−6.0 Hz for $^2J_{C3,H2R}$ and −1.5 Hz for $^2J_{C3,H2S}$) determined from data in Figure 13C assuming the $E_2/{}^4T_3$ conformational model derived from $^3J_{HH}$ treatment (Table 2).

$^2J_{C3,H4}$ is essentially the same in **5** and **6** (∼ −5.5 Hz). This coupling is predicted to be negative in all ring conformations and relatively insensitive to ring conformation (Figure 9E). $^2J_{C4,H3}$ is 1.5 Hz (sign uncertain) in **6** and −0.7 Hz in **5**. Data in Figure 9F indicate that conformational averaging in **6** ($E_2/{}^4T_3$) and in **5** ($E_2/{}^2E$) will yield a more positive (less negative) coupling for **6** than for **5**. We thus expect $^2J_{C4,H3}$ in **6** to be positive in sign. In comparison, $^2J_{C4',H3'}$ values of +2−5 Hz have been observed in residues of an RNA oligomer that prefer S conformations and values of − ∼2.6 Hz in residues that prefer N forms.[19] Thus, the larger percentage of S forms in **6** should result in a less negative (more positive) $^2J_{C4,H3}$ value than observed in **5**.

Three-Bond $^{13}C-{}^1H$ Couplings. $^3J_{C1,H3}$ in **5** is considerably smaller (1.2 Hz) than that in **6** (2.7 Hz). Data in Figure 11A show that the dependence of this coupling on ring conformation is similar in both compounds. Thus, the larger value observed in **6** suggests a larger percentage of S forms in solution, since this coupling increases in magnitude as the proportion of S forms increases. This result is consistent with conclusions drawn from the treatment of $^3J_{HH}$ data (Table 2). $^3J_{C1,H3}$ in **5** (1.2 Hz) is considerably smaller than $^3J_{C1',H3'}$ in ribonucleosides (3.0−5.1 Hz),[43] suggesting a greater proportion of S forms in the latter, again consistent with $^3J_{HH}$ data.[61] $^3J_{C1,H3}$ in **6** (2.7 Hz) is considerably smaller than $^3J_{C1',H3'}$ in 2′-deoxyribonucleosides (4.5−5.3 Hz),[60] which is consistent with the larger percentage of S forms in the latter indicated by $^3J_{HH}$ analysis.[61] By comparison, $^3J_{C1',H3'}$ values of ∼6.6 Hz have been reported in residues of RNA oligomers that highly prefer S forms.[19]

$^3J_{C1,H4}$ in **5** (2.9 Hz) is smaller than that in **6** (4.8 Hz). Inspection of Figure 11B shows essentially the same dependence on ring conformation in both compounds. Thus, the larger value observed in **6** indicates a larger proportion of S forms relative to **5**. Interestingly, $^3J_{C1',H4'}$ in ribonucleosides[43] and 2′-deoxyribonucleosides[60] are <1.3 and <2.9 Hz, respectively, that is, considerably smaller than corresponding values in **5** and **6**. This result suggests that different N and S forms are involved in the N/S equilibria of **5**, **6**, ribonucleosides, and 2′-deoxyribonucleosides. Inspection of Figure 11B shows that N/S equilibria involving ^3E and ^2E forms (the conventional model for N/S exchange) would result in a small observed $^3J_{C1',H4'}$ value, since couplings < ∼2.5 Hz are associated with these forms. On the other hand, the $E_2/{}^2E$ and $E_2/{}^4T_3$ conformational equilibria proposed for **5** and **6**, respectively (Table 2), would produce considerably larger $^3J_{C1,H4}$ values, as observed.

$^3J_{C2,H4}$ = 0.9 Hz for **5** and ∼1.2 Hz for **6**. $^3J_{C2',H4'}$ values are <1.6 Hz in ribonucleosides[43] and <1.1 Hz in 2′-deoxyribonucleosides.[60] These couplings are very similar for compounds having considerably different conformational properties, suggesting that $^3J_{C2,H4}$ is not a sensitive conformational probe in *β*-D-*ribo* and 2-deoxy-*β*-D-*ribo* rings. The complex response of this coupling to conformation (Figure 11D) and/or the relatively small range of values for this coupling (< ∼4 Hz for **4**, < ∼2 Hz for **3**) are responsible for this insensitivity. Interestingly, $^3J_{C2',H4'}$ values of 0.3−1.6 Hz have been observed in residues of RNA oligomers that prefer N forms,[19] again small as found in **5**.

The similar values of $^3J_{C3,H1}$ in **5** (3.1 Hz) and **6** (3.3 Hz) are consistent with the conformational models based on $^3J_{HH}$ analysis (Table 2). For **5**, weighted averaging of the $E_2/{}^2E$ model predicts a value of ∼2.4 Hz, whereas similar averaging for **6** ($E_2/{}^4T_3$ model) yields a value of ∼2.5 Hz (Figure 11E). By comparison, values of 0.6 Hz have been observed in residues of RNA oligomers that prefer S forms.[19]

$^3J_{C4,H1}$ is slightly larger in **6** (5.0 Hz) than in **5** (4.5 Hz). The favored N forms of both compounds (E_2) are predicted to yield similar couplings (Figure 11C), whereas the preferred S form of **6** ($^4T_3$) should give a larger coupling than the preferred S form of **5** (^2E). Conformational averaging (data in Figure 11C and N/S data in Table 2) yields a coupling that is 0.7 Hz larger in **6** (5.6 Hz) than in **5** (4.9 Hz), in good agreement with the observed difference (0.5 Hz). Given the nature of the $^3J_{C4,H1}$/ring conformation curve (Figure 11C), this coupling will not be highly sensitive to conventional N/S exchange (*i.e.*, $^3E/{}^2E$), since $^3J_{C4,H1}$ is small in these two conformers (<3 Hz).

$^3J_{C4,H2}$ is ∼4.3 Hz in **5** and $^3J_{C4,H2S}$ is 4.2 Hz in **6**. Data in Figure 11F show similar dependencies on ring conformation, and conformational averaging is expected to lead to similar values of these couplings (4.2 and 3.6 Hz, respectively). By comparison, $^3J_{C4',H2'}$ values range from 3.8−5.8 Hz in residues of RNA oligomers preferring N forms.[19] In **6**, $^3J_{C4,H2R}$ = 2.0 Hz, which is considerably smaller than $^3J_{C4,H2S}$. These paired couplings are expected to exhibit complementary behavior, with $^3J_{C4,H2S} > {}^3J_{C4,H4R}$ for N conformers and $^3J_{C4,H2S} < {}^3J_{C4,H2R}$ for S conformers (Figure 13D). The N/S model for **6** based on $^3J_{HH}$ analysis (Table 2) and data in Figure 13D lead to the

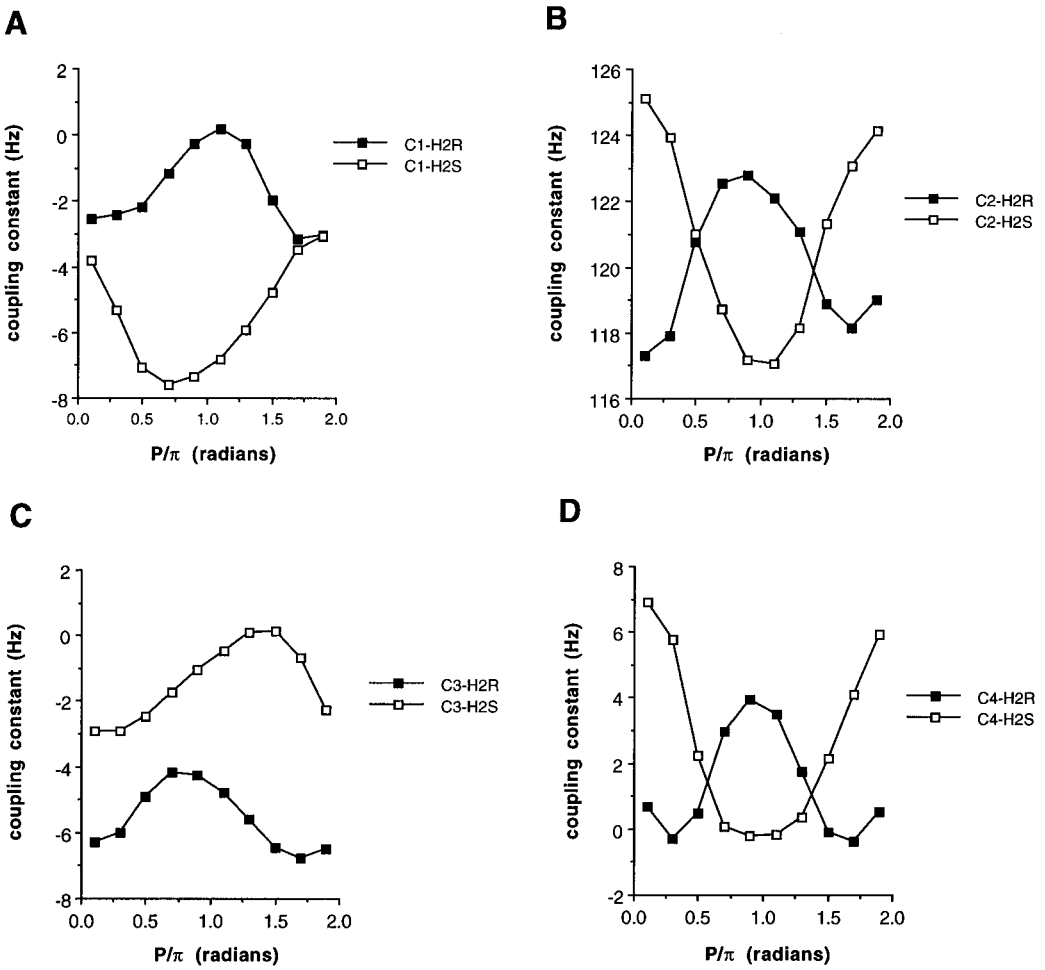

Figure 13. Computed J_{CH} values involving H2*R* and H2*S* in **3** determined from *ab initio* molecular orbital calculations (HF/6-31G*).

prediction that $^3J_{C4,H2S}$ should be ~2.3 Hz larger than $^3J_{C4,H2R}$, in good agreement with observation.

$^3J_{C5,H3}$ values in **5** and **6** are similar (~4.8 and 4.0 Hz, respectively), and the smaller value observed in **6** is consistent with $^3J_{HH}$ conformational models (this effect is attributed to the different preferred S forms of **5** and **6**, in which the C5−C4−C3−H3 dihedral angle is slightly larger for **6** than for **5**). Previous studies of $^3J_{C5,H3}$ in the *β*-D-*ribo* ring suggested that this coupling might not be useful to assess conformational exchange due to its limited sensitivity to conformation.[28] This conclusion was based on the extrapolation of Karplus behavior reported for C−C−C−H coupling pathways in carbohydrates[58a] for dihedral angles of ±40° (Figure 10). However, the computed behavior of $^3J_{C5,H3}$ in **3** and **4** determined in this study (Figure 14A) differs considerably from that reported previously,[28] and we attribute this discrepancy to faulty extrapolation of coupling constants at the smaller dihedral angles. The computed data (Figure 14A) reveal a moderate dependence of $^3J_{C5,H3}$ on ring conformation in **3** and **4**, with values ranging from ~1.5−5.5 Hz. It is interesting to note that the computed dependence of $^3J_{C5,H3}$ on dihedral angle is not symmetric about 0° (Figure 14B), at least for conformers having the *gt* conformation about the C4−C5 bond. This behavior results in the loss of the expected biphasic behavior in Figure 14A for this cisoidal coupling.

One-Bond ^{13}C−^{13}C Couplings. $^1J_{C1,C2}$ in **5** (46.8 Hz) is smaller than $^1J_{C1,C2}$ in **6** (40.5 Hz). The difference (Δ = 6.3 Hz) is similar to that observed between ribonucleosides and 2′-deoxyribonucleosides (Δ = ~5.9 Hz)[43,60,61] and is attributed mainly to the loss of an electronegative substituent on one of the coupled carbons. Interestingly, $^1J_{C1',C2'}$ averages 42.8 ± 0.2 Hz in ribonucleosides[43] and 36.9 ± 0.3 Hz in 2′-deoxyribonucleosides,[61] values which are ~4 Hz smaller than corresponding values in **5** and **6**. The less electronegative nitrogen at C1′ in the nucleosides (relative to oxygen in **5** and **6**) is probably responsible for the smaller $^1J_{C1',C2'}$ in nucleosides.

$^1J_{C2,C3}$ is 1.8 Hz larger in **5** (37.2 Hz) than in **6** (35.4 Hz), and this difference is similar to that observed between ribonucleosides and 2′-deoxyribonucleosides (~2.2 Hz).[61] These couplings are also similar in magnitude to those observed in ribonucleosides (37.8 ± 0.1 Hz)[43] and 2′-deoxyribonucleosides (35.6 ± 0.1 Hz).[61]

$^1J_{C3,C4}$ is slightly larger in **5** than in **6**; corresponding values in nucleosides have not yet been reported. Interestingly, $^1J_{C4,C5}$ is similar in **5** and **6** (42.0 Hz and 41.5 Hz, respectively) and is considerably larger than $^1J_{C2,C3}$ and $^1J_{C3,C4}$ values despite similar substitution patterns on the C−C fragment. Similar enhanced couplings have been observed in the exocyclic C5−C6 fragment of aldopyranosyl rings.[68]

Two-Bond ^{13}C−^{13}C Couplings. The three *intraring* two-bond ^{13}C−^{13}C spin-couplings in **5** and **6** ($J_{C1,C3}$, $J_{C1,C4}$, $J_{C2,C4}$) are dual pathway couplings (*i.e.*, $^{2+3}J_{CC}$); for example, $J_{C1,C3}$ is governed by the C1−C2−C3 and C1−O4−C4−C3 coupling pathways. $^{2+3}J_{C1,C4}$ is essentially zero in **5** and **6**; $^{2+3}J_{C1',C4'}$ in ribonucleosides is <0.9 Hz[43] and appears to be only slightly larger in 2′-deoxyribonucleosides.[61] $^{2+3}J_{C2,C4}$ values are also essentially the same in **5** and **6** (~1.2 Hz); corresponding values in ribo- and 2′-deoxyribonucleosides are 0.4−1.0[43] and ~0 Hz,[61] respectively. These results suggest that $^{2+3}J_{C1,C4}$ and $^{2+3}J_{C2,C4}$ are not particularly sensitive to differences in the conformational behavior of *β*-D-*ribo* and 2-deoxy-*β*-D-*ribo* rings.

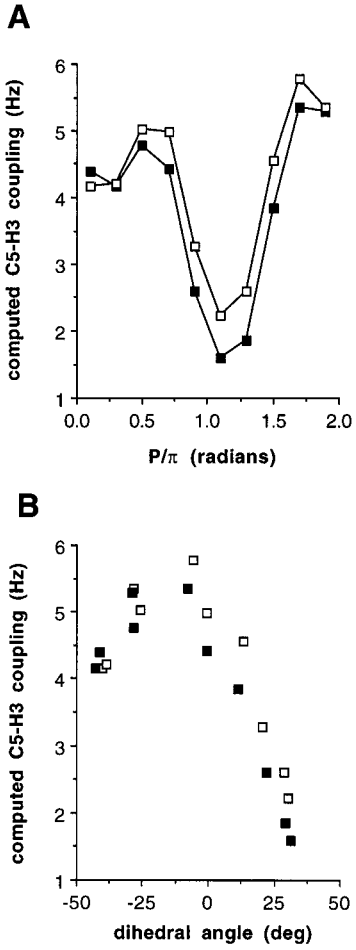

Figure 14. (A) Computed $^{3}J_{C5,H3}$ values in **3** (open squares) and **4** (closed squares) as a function of ring conformation. (B) Effect of the C5−C4−C3−H3 dihedral angle on $^{3}J_{C5,H3}$ magnitude (**3**, open squares; **4**, closed squares).

In contrast to $^{2+3}J_{C1,C4}$ and $^{2+3}J_{C2,C4}$, $^{2+3}J_{C1,C3}$ is significantly different in **6** (<0.8 Hz) and **5** (3.0 Hz), and the latter is probably positive in sign.[61] Corresponding values in ribo- and 2′-deoxyribonucleosides are 3.3−3.8[43] and 0.8 Hz,[61] respectively, which are similar to those observed in **5** and **6**, respectively. We have shown recently that $^{2+3}J_{C1,C3}$ is insensitive to ring conformation and that the difference observed between *β*-D-*ribo* and 2-deoxy-*β*-D-*ribo* rings is due to substitution effects along the two-bond (C1−C2−C3) coupling pathway.[61] The fact that similar couplings are observed in **5** and ribonucleosides and **6** and 2′-deoxyribonucleosides, despite differences in conformational behavior, provides additional support for this explanation. The smaller couplings observed in **5** and **6** relative to those observed in the corresponding nucleosides may be caused by substitution effects at C1 (N *vs* O).

$^{2}J_{C1,OCH_3}$ in **5** and **6** are 2.0 and 1.8 Hz, respectively (Table 4). These values are probably negative in sign, as predicted by the projection resultant method,[13,29] and are expected in two C1−O1 rotamers, namely, those having CH_3 *gauche* to H1 and O4 and CH_3 *gauche* to C2 and O4. The remaining C1−O1 rotamer (CH_3 *gauche* to H1 and C2) is predicted to give a small or zero value for $^{2}J_{C1,OCH_3}$.[13] Therefore, the data suggest that the latter rotamer is not highly populated in **5** and **6**. The relatively large magnitudes of $^{3}J_{C2,OCH_3}$ in **5** and **6** (see Discussion below) further suggest that, of the two possible preferred rotamers, that having CH_3 *gauche* to H1 and O4 is more favored.

$^{2}J_{C3,C5}$ values in **5** and **6** are 2.3 and 3.6 Hz, respectively (Table 4) and probably have a positive sign.[13] These couplings will be affected by ring conformation and hydroxymethyl group conformation (C4−C5 torsion). Previous analyses of $^{2}J_{C3,C5}$ in pentofuranose rings[68] led to the prediction that this coupling should be relatively large in conformers near ^{4}E for D-ribo- and D-arabinofuranosyl rings in which the *gt* conformation about the C4−C5 bond (O5 *gauche* to H4 and O4) is favored. Indeed, in *β*-D-ribofuranose, $^{2}J_{C3,C5}$ = 1.8 Hz.[68] $^{2}J_{C3,C5}$ in **5** is considerably smaller than $^{2}J_{C3,C5}$ in **6**, and this difference is not expected to arise from differences in substitution at C2. The preferred conformation of **5** is E_2 (N form, 94%), whereas **6** prefers comparable proportions of N (E_2) and S ($^{4}T_3$) forms (60/40) (Table 2). Furthermore, the *gt* conformation is equally populated in **5** and **6** (Table 3). Therefore, the larger $^{2}J_{C3,C5}$ value observed in **6** may be attributed to the enhanced proportion of the $^{4}T_3$ form in solution, which is similar in structure to ^{4}E (Chart 1) (we assume here that the differences in the *gg* and *tg* populations in **5** and **6** (Table 3) do not significantly affect the observed $^{2}J_{C3,C5}$ values). These results suggest that $^{2}J_{C3,C5}$

Table 6. Changes in J_{CH} Values Predicted by *ab Initio* Methods for 2-Deoxy-*β*-D-ribofuranose **3** and *β*-D-ribofuranose **4**

coupling	full itinerary[a]	^{3}E/^{2}E model[b]
	2-Deoxy-*β*-D-*ribo* **3**	
C1−H1	10.0	4.5
C2−H2*R*	5.5	5.5
C2−H2*S*	8.1	7.9
C3−H3	4.2	2.7
C4−H4	8.1	5.0
C1−H2*R*	3.3	2.3
C1−H2*S*	4.5	3.5
C2−H1	**1.7**	**0.2**
C2−H3	2.9	**1.4**
C3−H2*R*	2.6	2.0
C3−H2*S*	3.0	**1.9**
C3−H4	**1.1**	**0.6**
C4−H3	5.6	4.7
C1−H3	6.5	6.5
C1−H4	8.7	2.7
C2−H4	2.6	**0.8**
C3−H1	4.1	2.4
C4−H1	7.6	2.5
C4−H2*R*	4.4	3.3
C4−H2*S*	7.1	7.1
C5−H3	3.6	**0.9**
	β-D-*ribo* **4**	
C1−H1	9.6	4.4
C2−H2	11.1	10.1
C3−H3	4.5	**1.8**
C4−H4	9.7	5.5
C1−H2	7.5	6.4
C2−H1	**1.4**	**0.5**
C2−H3	2.5	**0.4**
C3−H2	2.8	2.3
C3−H4	**1.8**	**1.0**
C4−H3	7.3	5.7
C1−H3	5.8	5.8
C1−H4	7.6	**1.6**
C2−H4	4.1	**0.9**
C3−H1	3.2	**1.5**
C4−H1	7.7	**1.4**
C4−H2	5.3	5.0
C5−H3	3.8	**1.8**

[a] Maximum change in coupling over the full pseudorotational itinerary. [b] Change predicted for a two-state ^{3}E/^{2}E exchange model. Values <2 Hz are indicated in bold; these couplings are considered to be of limited value in conformational analysis.

(66) Varani, G.; Tinoco, I., Jr. *J. Am. Chem. Soc.* **1991**, *113*, 9349−9354.
(67) Kline, P. C.; Serianni, A. S. *J. Org. Chem.* **1992**, *57*, 1772−1777.
(68) Wu, J.; Bondo, P. B.; Vuorinen, T.; Serianni, A. S. *J. Am. Chem. Soc.* **1992**, *114*, 3499-3505.

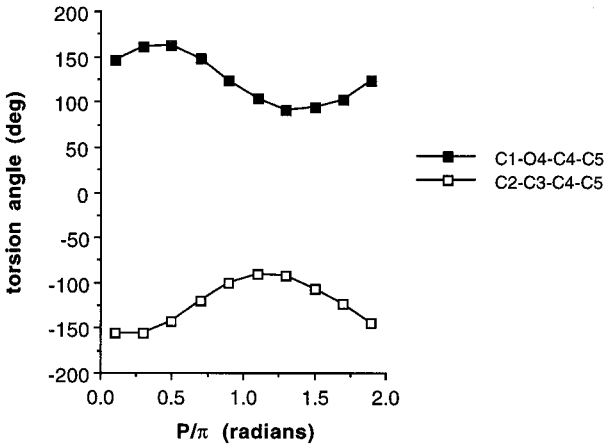

Figure 15. Effect of ring conformation on the two C−C torsion angles involving C5 of **3** determined from *ab initio* molecular orbital calculations (HF/6-31G*). Corresponding data for **4** are essentially the same.

should be further explored as a probe of furanose N/S conformation in DNA and RNA, since hydroxymethyl conformation in these biopolymers is constrained (*gg* conformation), thus making ring conformation the only key determinant.[69]

Three-Bond ^{13}C−^{13}C Couplings. $^3J_{C1,C5}$ is very small in both **5** and **6** (<0.8 Hz); corresponding values in ribonucleosides and 2′-deoxyribonucleosides are 0−1.8[43] and ∼0.8 Hz,[61] respectively. Considering the effect of ring conformation on the C1−O4−C4−C5 torsion angle (Figure 15), the N/S conformational model for **5** is predicted to produce a coupling similar to (or perhaps slightly larger than) that observed in **6**; this coupling, however, will be very small, since torsion angles of 90°−125° are involved. $^3J_{C1,C5}$ is expected to be large in E_4 and ^{0}E forms (dihedral angles of ∼160°) and small in ^{4}E and E_0 forms (dihedral angles of ∼90°).

$^3J_{C2,C5}$ is 1.8 Hz in **5**. Corresponding values in pyrimidine ribonucleosides (pyrR) and purine ribonucleosides (purR) are 1.6 and ∼0 Hz, respectively.[43] This coupling is expected to increase in magnitude as N forms become more favored, based on the effect of ring conformation on the C2−C3−C4−C5 torsion angle (Figure 15). $^3J_{HH}$ data suggest that % N forms in solution decreases in the order **5** > pyrR > purR, and $^3J_{C2,C5}$ values reflect this trend.

$^3J_{C2,C5}$ is 1.1 Hz in **6**; in contrast, values of 1.3 and ∼0 Hz are observed in pyrimidine 2′-deoxyribonucleosides (pyrDR) and purine 2′-deoxyribonucleosides (purDR), respectively.[61] $^3J_{HH}$ data suggest that % N forms in solution decreases in the order pyrDR ≈ **6** > purDR, and $^2J_{C2,C5}$ data are in accord with this trend.

$^3J_{C2,OCH_3}$ in **5** and **6** are 3.5 and 3.0 Hz, respectively (Table 4). These three-bond couplings are related to $^3J_{C1,C6}$ in aldopyranosides, since both involve a C−O−C−C coupling pathway. In D-aldopyranosides having the $^4C_1$ conformation, $^3J_{C1,C6}$ varies from 3.3−4.5 Hz.[68,70] The latter couplings are

(69) The application of the projection resultant method[13] to $^2J_{C3,C5}$ in **5** and **6** yields predictions regarding the sensitivity of this coupling to ring and hydroxymethyl conformation. For $^3E/E_4$ conformers (N forms), predicted $^2J_{C3,C5}$ values are ∼ −2 Hz (*gg*), 0−1 Hz (*gt*), and ∼ −2 Hz (*tg*); for $E_3/^4E$ conformers (S forms), these couplings are 0−1, 3−4, and 0−1 Hz, respectively. While these predicted *J* values cannot be considered accurate (the method was devised for C−C−C coupling pathways involving nonterminal coupled carbons), the trends are probably reliable. Thus, for example, the $E_3/^4E$ (*gt*) conformer is predicted to yield a more positive coupling than $E_3/^4E$ (*gg*) and $E_3/^4E$ (*tg*) conformers, which is consistent with previous empirical predictions (in the former conformations, both O3 and O5 lie in the C3−C4−C5 plane).[68] Furthermore, considerable differences in coupling are predicted depending on ring and hydroxymethyl group conformation (*e.g.*, ∼5−6 Hz between $^2J_{C3,C5}$ in $^3E/E_4$ (*gg*) and $E_3/^4E$ (*gt*)). In oligonucleotides where hydroxymethyl conformation is fixed in the *gg* rotamer, $^2J_{C3,C5}$ may differ by as much as 3 Hz between N and S forms, although the extent of the difference will be influenced by the preferred N and S forms (*e.g.*, $^3E/^2E$ exchange may be accompanied by a smaller difference in $^2J_{C3,C5}$ values than $E_4/^4E$ exchange).

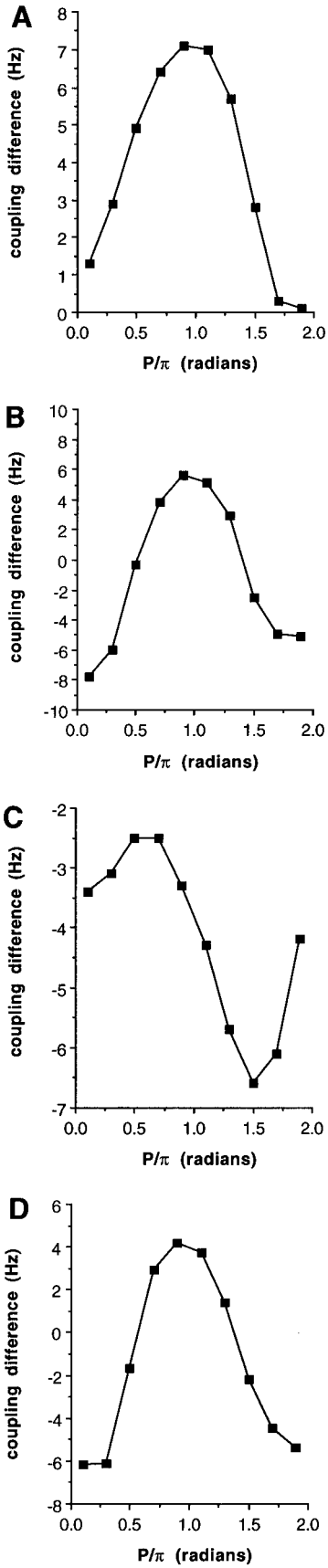

Figure 16. Coupling difference plots for J_{CH} values involving H2*R* and H2*S* of **3**: (A) $^2J_{C1,H2R} - {}^2J_{C1,H2S}$, (b) $^1J_{C2,H2R} - {}^1J_{C2,H2S}$, (C) $^2J_{C3,H2R} - {}^2J_{C3,H2S}$, and (D) $^3J_{C4,H2R} - {}^3J_{C4,H2S}$.

associated with a C−O−C−C dihedral angle of ∼180°; the observed range of values is apparently caused mainly by the effects of terminal hydroxyl group orientation (O1 and O6) on coupling magnitude (α-substituent effects), although small deviations from ideal chair geometry in different ring configurations may also make a contribution.[68] Based on these data, the observed values of $^3J_{C2,OCH_3}$ in **5** and **6** are consistent with a preferred C2−C1−O−CH_3 dihedral angle approaching 180°, which orients the methyl carbon *gauche* to O4 and H1. This arrangement is consistent with expectations based on stereoelectronic considerations (exoanomeric effect[53]). It should be appreciated, however, that the coupling pathways governing $^2J_{C2,OCH_3}$ in **5** and **6**, and indeed the reference C1−O5−C5−C6 pathway in aldopyranosyl rings, are not similarly substituted. For example, only one of the coupled carbons (C2) is substituted with an electronegative atom in **5**, whereas none are in **6**. This substitution effect alone could cause the 0.5 Hz difference in $^3J_{C2,OCH_3}$ values observed between **5** and **6**, that is, this difference may not reflect different C1−O1 torsional behavior. Thus, given these limitations, the above C1−O1 conformational conclusions based on $^3J_{C1,C6}$ reference values must be viewed with appropriate caution.

Conclusions

Three-dimensional structure determination of nucleic acids has benefited greatly from the use of ^{13}C- and ^{15}N-enrichment, which permits the application of multidimensional heteronuclear NMR methods required for spectral dispersion and signal assignment. ^{13}C-enrichment also permits the determination of ^{13}C−^{1}H and ^{13}C−^{13}C spin-couplings within the furanose rings and across the *N*-glycosidic linkages of these structures which are potentially useful as conformational probes. In the present investigation, we have compared the behaviors of one-, two-, and three-bond ^{13}C−^{1}H and ^{13}C−^{13}C spin-coupling constants within *β*-D-*ribo* **1** and 2-deoxy-*β*-D-*ribo* **2** rings. Computational approaches were applied in an effort to assess the effect of C2 substitution (oxy *vs* deoxy) on the magnitudes and signs of J_{CH} values. In a previous report, J_{CH} behavior in *β*-D-*ribo* rings was examined using similar calculational methods, and the latter were validated by measuring J_{CH} values in conformationally-constrained aldopyranosyl rings containing coupling pathways that mimic those found in discrete conformations of this ring.[28] The results of this prior work showed that, while the *absolute values* of the couplings predicted by the computations cannot be considered accurate, the *trends* were reliable. Since the present study relies mainly on trends rather than on absolute values, we did not consider it necessary to prepare a wide range of model deoxypyranoses to further validate the method, although couplings in a few model compounds have been examined. Indeed, comparisons between related couplings within the furanose constituents of oligonucleotides can yield important information on conformational differences, since all furanosyl rings within natural oligomers will have the same chemical structure. Model compounds will be required, however, in future studies of absolute coupling magnitudes.

It should be appreciated that, due to present computer limitations, only one set of exocyclic torsion angles in **3** and **4** was inspected in this work. The C1−O1 torsions were chosen to maximize the exoanomeric effect,[53] and the *gt* conformation about the C4−C5 bond was selected because both **5** and **6** favor this conformation (Table 3). The remaining exocyclic C−O torsions were chosen arbitrarily. Thus, conformational energy data shown in Figure 1 represent a small portion of the total energy surface available to **3** and **4**, and thus these data must be viewed with appropriate reservation; this limitation is confirmed by computations conducted on **6** using the Consistent Force Field method which show that exocyclic C−O and C−C torsions indeed affect conformational energies.[71] Similar limitations apply to the observed structural trends (*i.e.*, bond lengths, bond angles, bond torsions).

Extrapolation of the present results to coupling behavior in oligonucleotides assumes that the preferred *gg* conformation about the C4′−C5′ bond in these structures does not significantly affect coupling behavior. The latter assumption is probably valid for coupled nuclei within the furanose ring. On the other hand, couplings such as $^2J_{C3,C5}$, $^3J_{C1,C5}$, $^3J_{C2,C5}$, and $^3J_{C5,H3}$ may be affected by the orientation of the terminal oxygen on C5 with respect to the coupling pathway (α-substituent effects). ^{13}C−^{1}H couplings involving H5*R* and H5*S* are also affected by the C4−C5 torsion angle, but their dependence can be predicted qualitatively, as discussed in this report. Furthermore, direct application of this study to oligonucleotides assumes that *O*-phosphorylation (at O3 and O5) does not affect J_{CH} or J_{CC} behavior significantly. The validity of this assumption remains to be tested with the use of suitable model sugar phosphates.

Observed J_{CH} values in **5** and **6** were interpreted in structural and conformational terms in this work with the use of computed couplings and/or the application of the projection rule[64] (for $^2J_{CH}$). In most cases, both tools gave internally consistent results which led to reasonable interpretations of the observed coupling data. However, in two cases, namely, $^2J_{C2,H3}$ (Figure 9D) and $^3J_{C2,H4}$ (Figure 11D), discrepancies were observed, and these findings require further scrutiny. Furthermore, the application of the projection rule,[64] which was developed for C−C−H coupling pathways involving hydroxylated carbons, may not be appropriate for the analysis of $^2J_{CCH}$ values involving C2 of the 2-deoxy-*β*-D-*ribo* ring; this problem will need to be addressed by examining $^2J_{CCH}$ values in deoxysugars having defined conformations (*e.g.*, deoxypyranosyl rings).

Despite the above-noted limitations, however, a number of observations have been made which have important implications for the anticipated use of J_{CH} and J_{CC} values as conformational probes in furanose rings.

(a) The behavior of $^1J_{CH}$ values in the 2-deoxy-*β*-D-*ribo* ring **2** is consistent with previous observations on the relationship between C−H bond orientation and $^1J_{CH}$ coupling magnitudes in the 2-deoxy-*β*-D-*glycero*-tetrofuranose[27] and *β*-D-ribofuranose rings.[28] C−H bond orientation appears to play an important role in determining $^1J_{CH}$ values, with quasi-equatorial orientations giving larger couplings than quasi-axial orientations for a given C−H bond. However, at least two additional factors affect C−H bond length, and thus $^1J_{CH}$ values, in these rings. Vicinal lone-pair effects (*e.g.*, the interaction of lone-pair orbitals on O3 with the C3-H3 bond) appear to be substantial, with antiperiplanar arrangements causing *bond lengthening* as reported previously.[27,28,50−52] In addition, recent studies[72] suggest that 1,3-interactions between oxygen lone-pair orbitals and C−H bonds (*e.g.*, the interaction of lone-pair orbitals on O3 with the C4−H4 bond) also affect C−H bond lengths in a consistent fashion. These latter interactions, when present, appear to cause *bond shortening*, and this effect is discussed in a recent report.[72] Thus, it appears that C−H bond orientation, while important, may not be the sole determinant of C−H bond length in aldofuranosyl rings.

(70) King-Morris, M. J.; Serianni, A. S. *J. Am. Chem. Soc.* **1987**, *109*, 3501−3508.

(71) Wiorkiewicz-Kuczera, J.; Rabczenko, A. *J. Chem. Soc. Perkin Trans. II* **1986**, 437-442.

(72) Kennedy, J.; Wu, J.; Drew, K.; Carmichael, I.; Serianni, A. S. *J. Am. Chem. Soc.* In press.

(b) Exocyclic bonds other than C−H bonds (*e.g.*, C2−O2, C3−O3, and C4−C5 bonds) are also sensitive to bond orientation, again with quasi-axial orientations correlated with longer bonds and quasi-equatorial orientations correlated with shorter bonds (Figure 4A,B; Figure 6). This predicted (computed) behavior is consistent with recent analyses of X-ray crystallographic data on >100 nucleosides and nucleotides reported by Berman and co-workers.[56] This latter study shows that the mean values of the C2′−O2′ bond length in β-D-*ribo* rings **1** are 1.412 Å in ^{2}E (shorter, quasi-equatorial) and 1.420 Å in ^{3}E forms (longer, quasi-axial), whereas the mean values of the C3′−O3′ bond are 1.427 and 1.417 Å for ^{2}E (longer, quasi-axial) and ^{3}E forms (shorter, quasi-equatorial), respectively. In 2-deoxy-β-D-*ribo* rings **2**, the mean C3′−O3′ bond length is 1.435 Å in ^{2}E (longer, quasi-axial) and 1.419 Å in ^{3}E (shorter, quasi-equatorial) forms. The C3′−O3′ bond lengths in **2** are also, on average, longer than those observed in **1**, again in agreement with computed behavior (Figure 4B). Furthermore, the computed behavior of the endocyclic C1−O4 and C4−O4 bonds in *ribo* and deoxy*ribo* rings ($r_{C1-O4\ (ribo)} < r_{C1-O4\ (deoxyribo)}$ and $r_{C4-O4\ (ribo)} > r_{C4-O4\ (deoxyribo)}$) (Figure 5A,B) is in accord with crystallographic results (mean C1′−O4′ values are 1.415 Å (*ribo*) and 1.420 Å (deoxy*ribo*) for ^{2}E forms and 1.412 Å (*ribo*) and 1.418 Å (deoxy*ribo*) for ^{3}E forms, whereas mean values of C4′−O4′ are 1.454 Å (*ribo*) and 1.446 Å (deoxy*ribo*) for ^{2}E forms and 1.451 Å (*ribo*) and 1.449 Å (deoxy*ribo*) for ^{3}E forms). While the behavior of the C1−O4 and C4−O4 bond lengths may depend on the nature of the substituent at C1 (nitrogen base *vs* OH), it is less likely that this substituent change will significantly affect the behavior of the C2−O2 and C3−O3 bond lengths. Thus, we interpret the observed agreement between the computed and crystallographic behavior of the *exocyclic* C−O bond lengths as evidence, albeit indirect, that the correlations between C−H bond length and C−H bond orientation are valid, although experimental support for the latter remains to be obtained.

(c) Deoxygenation at the C2 position of a β-D-ribofuranosyl ring can, in some instances, result in substantial changes in the behavior of J_{CH} values within the ring. $^1J_{C1,H1}$ and $^1J_{C4,H4}$ appear to be essentially unaffected (Figure 8A,D), whereas $^1J_{C2,H2S}$ and $^1J_{C3,H3}$ are shifted to smaller values in the deoxy*ribo* ring (Figure 8B,C) . Likewise, $^2J_{C1,H2S}$, $^2J_{C3,H2S}$, and $^2J_{C4,H3}$ are less positive (more negative) in the deoxy*ribo* ring (Figure 9A,B,F), whereas the opposite is predicted for $^2J_{C2,H1}$ and $^2J_{C2,H3}$ (Figure 9C,D). The latter results suggest that, for a two-bond C−C−H coupling pathway, the loss of an electronegative substituent on the carbon bearing the coupled hydrogen causes a shift to more negative (less positive) couplings, whereas the loss of an electronegative substituent on the coupled carbon causes a shift to more positive (less negative) couplings. The former observation is consistent with recent studies of $^2J_{C2,H1}$ values in simple furanoses, furanosides, and nucleosides; for example, in nucleosides which bear the less electronegative substituent at C1 (*i.e.*, nitrogen), $^2J_{C2,H1}$ is more negative by ∼2.5 Hz.[61]

(d) $^3J_{CH}$ behavior in β-D-*ribo* **1** and 2-deoxy-β-D-*ribo* **2** rings show essentially similar behavior except for $^3J_{C2,H4}$, which appears smaller in **2** in some conformations (Figure 11D). Small deviations observed for antiperiplanar arrangements (Figure 11) are attributed mainly to substituent effects[73] rather than differences in puckering amplitudes (Figure 7C).

(e) J_{CH} values in β-D-*ribo* **1** and 2-deoxy-β-D-*ribo* **2** rings exhibit different sensitivities to conformational change (Table 6). The two couplings that appear minimally affected by ring conformation are $^2J_{C2,H1}$ and $^2J_{C3,H4}$; these couplings are predicted to change by <2 Hz throughout the pseudorotational itinerary for both β-D-*ribo* and 2-deoxy-β-D-*ribo* rings (Table 6). $^3J_{C2,H4}$ may also be of limited use due to its more complex dependence on conformation (Figure 11D). The sensitivity of $^3J_{C5,H3}$ to ring conformation in **3** and **4** may be greater than previously expected;[28] this coupling may indeed be useful as a conformational probe in these ring configurations despite its cisoidal nature. Interestingly, the utility of J_{CH} values as conformational probes appears more restricted if a simple two-state ^{3}E/^{2}E exchange process is operating; under these conditions, nine of the 17 couplings listed in Table 6 show <2 Hz changes for the β-D-*ribo* ring, while six of the 21 couplings for the 2-deoxy-β-D-*ribo* ring show a <2 Hz change. Thus, in instances where a conventional ^{3}E/^{2}E exchange process occurs, a smaller number of J_{CH} values will be useful to assess the two populations.

2-Deoxy-β-D-*ribo* rings contain several paired C−H coupling pathways involving H2*R* and H2*S* (*e.g.*, C1−H2*R*/C1−H2*S*, C2−H2*R*/C2−H2*S*, C3−H2*R*/C3−H2*S*, C4−H2*R*/C4−H2*S*). The coupling behaviors of these paired pathways differ significantly (Figure 13), and these differences should prove useful to assess conformation, as illustrated in Figure 16. For example, $^1J_{C1,H2R}-{}^1J_{C1,H2S}$ ranges from 0−7 Hz (Figure 16A), whereas $^3J_{C4,H2R}-{}^3J_{C4,H2S}$ ranges ranges −6 to 4 Hz (Figure 16D).

(f) $^2J_{C4,H5R/S}$ values have been shown previously[19,65] to be useful parameters to assign the H5*R* and H5*S* signals in oligonucleotides where the C4−C5 bond rotamer is limited to the *gg* conformation. In this report, we have shown that $^2J_{C4,H5R/S}$ and $^3J_{C3,H5R/S}$, when applied in conjunction with $^3J_{H4,H5R/S}$ values, can be used to make similar assignments in furanosyl rings in general and to estimate the proportions of the *gg*, *gt*, and *tg* rotamers in solution. In addition, $^2J_{C5,H4}$ was found to be sensitive to C4−C5 bond rotation, being large and positive in the *gg* rotamer and small and negative in *gt* and *tg* rotamers (Table 5).

(g) $^2J_{C3,C5}$ values in β-D-*ribo* and 2-deoxy-β-D-*ribo* rings are affected by hydroxymethyl and ring conformation. Since hydroxymethyl conformation in oligonucleotides is limited to the *gg* rotamer, ring conformation is likely to be the most important determinant of its magnitude in these structures. In the latter regard, the application of the projection resultant method[13,69] predicts that conformations in which O3 lies in the coupling plane (*e.g.*, E_3/^{4}E) will give more positive couplings than when O3 lies out-of-plane (*e.g.*, ^{3}E/E_4), although this prediction will require experimental validation.

Acknowledgment. The research reported herein was supported by the Office of Basic Energy Sciences of the United States Department of Energy and Omicron Biochemicals, Inc. of South Bend, IN. This is Document No. NDRL-3974 from the Notre Dame Radiation Laboratory.

JA970231E

(73) Parella, T.; Sanchez-Ferrando, F.; Virgili, A. *Magn. Reson. Chem.* **1994**, *32*, 657−664.

(74) de Leeuw, F. A. A. M.; Altona, C. *J. Comp. Chem.* **1983**, *4*, 428.